# A simple model for the global surface warming pattern

Janine Flöter

February 4th, 2009

# Contents

# Abstract

There is a wide range of climate models that are used to gain knowledge about how the earth's climate system works and hor it will eventually change under perturbed external forcing scenarios. It is the aim of this work to develop a simple climate model that includes only the basic physics concerning the surface climate of the earth and then to use this model for experimental investigation of the interactions among various feedback mechanisms that control the climate response to a global warming scenario.

The 'fingerprint' of global surface warming is the land-sea contrast and the strong warming over the high latitudes of the northern hemisphere. Since this pattern is a robust result from all current general circulation model projections, one may assume that with a sufficient number of physical processes this pattern can be reproduced with a simple cconceptual climate model. Thus, the mechanisms that control the energy balance of te earth surface are implemented into the model. These are: solar and longwave radiation, sensible and latent heat flux and horizontal heat transport. A simple two-layer model is developed which can easily be integrated without high computational efforts or costs.

Several datasets from observational records and model outputs were used to come up with simple parameterizations for some of the modelled processes in the model. This is also documented in the following work.

The model will be test in different versions by combining the physical processes and concluding information from the response results. The impacts of the various feedback mechanisms were summarized in the current Fourth Assessment Report of the Intergovernmental Panel on Climate Change. Thus a comparison to these result is shown within this work.

# Chapter 1

# Introduction

A simple climate model, which is based upon elementary heat balance considerations, has been developed and used to study the effects of feedback processes on the main features of the global surface warming pattern induced by climatic changes.

As observations of surface temperatures in the 20th century have shown, the Earth's climate is currently experiencing a global warming trend, which is characterized by a certain global pattern of temperature change. This pattern, as can be seen in figure 1.1, is on the largest scale characterized by a land-sea contrast, whereby most land regions warm more than the surrounding oceans, and a pronounced polar amplification in surface warming, which often is attributed to snow and ice cover changes in that region. Certainly this warming pattern can somehow be pursued into the troposphere where integrated over the first 10 km of altitude the warming pattern is less pronounced than directly at the surface.

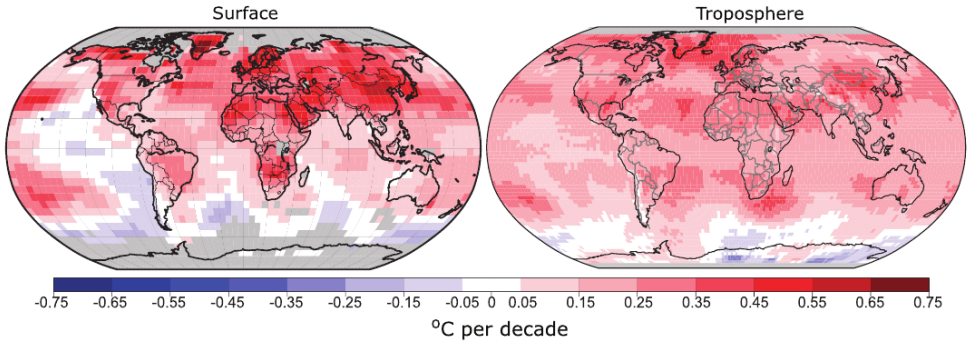


**fig.1.1** Patterns of linear global temperature trends from 1979 to 2005 estimated at the surface (left), and for the troposphere (right) from the surface to about 10 km altitude, from satellite records. Grey areas indicate incomplete data. Note the more spatially uniform warming in the satellite tropospheric record while the surface temperature changes more clearly relate to land and ocean.

Observed increases in the concentration of atmospheric carbon dioxide and other greenhouse gases are expected to have an important impact on climate and are assumed do be the primary driver of this warming trend on Earth. Thus scenarios of specific increases in greenhouse gas concentrations were used to calculate future climate projections in order to get insight into how climate change will further develop. As has already be shown by Sutton et al. (2007) these climate model simulations consistently show that in response to greenhouse gas forcing surface temperatures over land increase more rapidly than over

sea. This enhanced warming over land is not simply a transient effect, since it is always present in equilibrium conditions. The transient land-sea contrast is partially due to the contrast in heat capacity between the land and the ocean, with the latter mixing heat more readily away from the surface than the former. The polar amplification of surface temperature change, however, is not caused by this effect, since in polar regions sea ice dampens the effect of the difference in heat capacity between ocean and land. Thus, local feedback mechanisms and the hydrological cycle dominate the warming pattern, especially in equilibrium conditions, where the heat capacity has no impact.

The roboustness of current IPCC model results suggest a simple explanation. Here a simple argumentation based on the surface energy balance is presented. Without doubt, one must view with spekticism the numerical results obtained with a simple model, since the results are bound to be sensitive to the various parameterizations used to link the energy fluxes to surface temperature and other central variables of the model. However, as already discussed by North (1988) and Gal-Chen and Schneider (1975), it is remarkable that by employing a very simple formulation of the climate problem one seems to obtain quite good agreement with present climate predictions.

In order to set the developed simple climate model in context to the current scientific knowledge and to compare it with results from recent general circulation models, there will be a short summary of results of IPCC-AR4 in the following, which will be referred to in later sections of the work. Adjacent to this, a short overview over the hierarchy of climate models is given within the introduction. This shall give an impression of the role and potential of simple climate models. In chapter 2 the physical basis of the Earth's climate system will be described by introducing the different feedback processes, most of which will be implemented into the designed simple climate model. In chapter 3 the main aspects of natural as well as anthropogenically induced climatic change will be presented in order to define the scenario under which the model will be applied. The details of the simple model for the global surface warming pattern are described in chapter 4. In chapter 5 the results of various model experiments are presented and compared with the current IPCC results.

## 1.1 Summary of IPCC results

The response of simulated surface air temperature to greenhouse gas forcing was summarized in the Fourth Assessment Report of the Intergovernmental Panel of Climate Change [2007, further referred to as IPCC-AR4]. The projected warming in the 21st century shows scenario-independent geographical patterns similar to those observed over the past several decades. Figure 1.2 shows the ensemble mean pattern of surface warming for several time periods in the future. The greenhouse gas concentrations were assumed to follow the A1B scenario. The enhanced warming over land is clearly evident, as is the large warming at high northern latitudes. Minima in the Southern Ocean and North Atlantic Ocean are associated with large ocean heat uptake. The global land/sea warming ratio was determined to vary within the range of 1.36-1.84. The simulated polar amplification of surface warming is almost twice the global average and is generally attributed to snow and sea-ice albedo feedback, although recent studies suggest that other processes are also important.

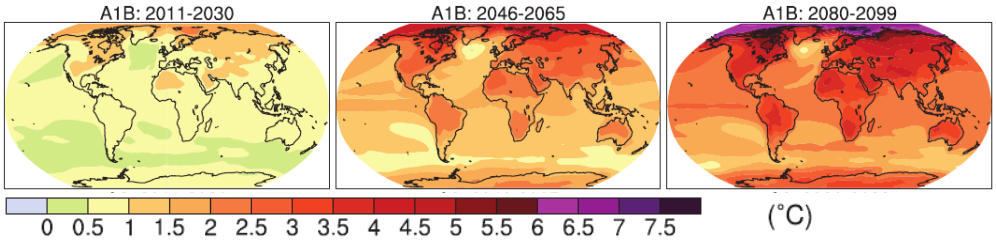


**fig.1.2** Multi-model mean of annual mean surface warming (surface air temperature change, °C) for the A1B scenario and three time periods, 2011 to 2030 (left), 2046 to 2065 (middle) and 2080 to 2099 (right). Anomalies are relative to the average of the period 1980 to 1999. (taken from IPCC-AR4)

The warming patterns for the early 21th century are remarkably similar to that at the end of the century. This indicates, that the warming pattern scales with the mean warming magnitude. However, the warming pattern is not homogeneous throughout the year. The amplified high-latitude warming is rather seasonal, being larger in winter as a result of sea ice and snow, as can been seen in figure 1.3.

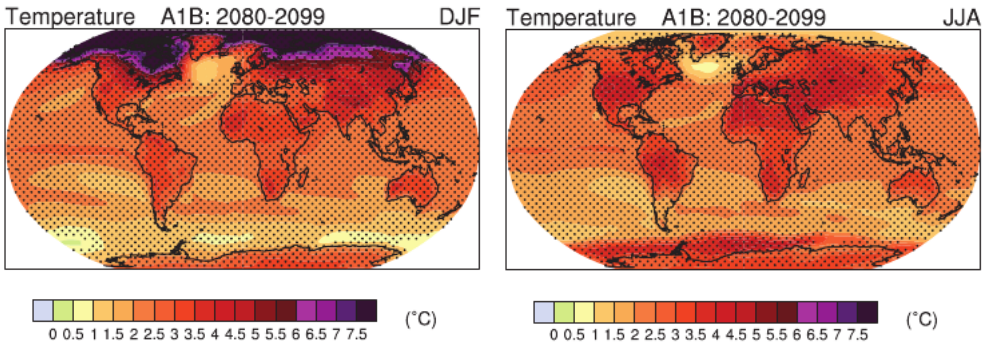


**fig.1.3** Multi-model mean change in surface temperature (°C) for boreal winter (DJF, left) and summer (JJA, right). Changes are given for the SRES A1B scenario, for the period 2080 to 2099 relative to 1980 to 1999. Stipping denotes areas where the magnitude of the multi-model ensemble mean exceeds the inter-model standard deviation.

Besides the changes in surface temperature there are changes in other parameters that also characterize the Earth's climate. Among those are the soilmoisture, which on the one hand is a reservoir for evaporation and on the other hand is a result of precipitation, and the energy fluxes which make up the surface energy balance, as there are: absorbed solar radiation, net (emitted minus received) longwave radiation, latent heat flux (associated with a flux of water vapor), and sensible heat flux.

As can be seen in figure 1.4, decreases in soilmoisture are common in the subtropics and the Mediterranean region. There are increases in east Africa, central Asia, and some other regions with increased precipitation. Decreases also occur at high latitudes, where snow cover diminishes. While the magnitudes of change are quite uncertain, there is good consistency in the signs of change in many of these regions. Annual average evaporation increases over much of the ocean, with spatial variations tending to relate to those in the surface warming.

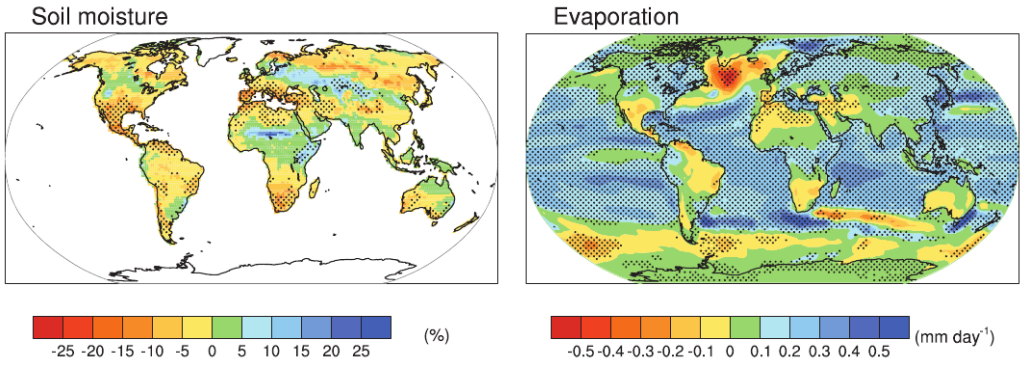


**fig.1.4** (left) Multi-model mean change in soil moisture (%). To indicate consistency in the sign of change, regions are stippled where at least 80% of models agree on the sign of the mean change. Changes are annual means for the SRES A1B scenario for the period 2080 to 2090 relative to 1980 to 1999. (right) Multi-model mean change in evaporation (mm/day). To indicate consistency in the sign of change, regions are stippled where at least 80% of models agree on the sign of the mean change. Changes are annual means for the SRES A1B scenario for the period 2080 to 2090 relative to 1980 to 1999.

According to IPCC-AR4 key uncertainties in future climate projections lay in the equilibrium climate sensitivity resulting from a given $CO_2$-equilibrium stabilisation scenario. Models differ considerably in their estimates of the strength of different feedbacks in the climate system, particularly cloud feedbacks, oceanic heat uptake and carbon cycle feedbacks, although progress has been made in these areas. Detecting, understanding and accurately quantifying climate feedbacks have been the focus of a great deal of research by scientists unravelling the complexities of Earth's climate.

## 1.2 Hierarchy of climate models

Mathematical models of climate are used to derive better understanding and allow some degree of predictive capability. According to Gal-Chen and Schneider (1975) and North (1975) climate models can be classified in a hierarchy generally based on geometric degrees of freedom ranging from globally-averaged vertical column models, which focus mostly on the radiative transfer properties of the atmosphere under various perturbations, and zonally averaged energy balance types, that allow latitude dependencies of albedo and surface temperature as well as meridional transfer of heat, to highly detailed three-dimensional global circulation models (GCMs) which might even incorporate circulation of the oceans and interactions with sea ice.

The simplest energy balance model (EBM) is the zero-dimensional model for annual mean global climate as has been developed and expanded by Budyko (1968) and Sellers (1969). The term EBM refers to those models that emphasize the calculation of surface temperature in terms of a balance between incoming solar and outgoing IR radiation. A review about these EBMs has been given by Schneider and Dickinson (1974), North et al. (1981) and North (1988). One appealing feature of the Budyko-Sellers models is their simplicity, which facilitates the use of the models as teaching tools. A somewhat higher position in the hierarchy is occupied by horizontally varying energy balance models. Additionally, in semiempirical models everything is parameterized in terms of surface temperature and its derivatives. Semiempirical models have the advantage that as their relative simplicity

they are inexpensive to run and their results are considerably easier to interpret physically than the larger more complex models.

At the next step, horizontal transport mechanisms are implemented into models. Adem (1970) assumed that latitudinal and longitudinal atmospheric and oceanic thermal transports may be parameterized largely in terms of horizontal 'Austausch' coefficients. Most recent versions of his model allow for transport by observed mean winds and by wind-driven ocean currents.

The most complex climate models are the high-resolution time-dependent general circulation models (GCMs) or even the atmosphere-ocean general circulation models (AOGCMs). One ultimate objective of mathematical models of climate is to include jointly all the coupled feedback processes in a realistic fashion. Models will become even more complex in future, including the effects of chemical and aerosol interactions with low-level cloud. Including a more comprehensive range of processes as well as an increase in the length of the simulations, and in spatial resolution improves the credibility of models in theory. Their major advantage (once perfected) will be their controllability, that is, the possibility of testing hypotheses by changing boundary conditions, a luxury not afforded by the real climate. Anyway, the models do not provide a perfect simulation of reality, because resolving all imortant spatial or time scales remains far beyond current capabilities. Details of atmospheric or oceanic processes on scales down to molecular motions will require a 'parameterization' of subgrid scale (often turbulent) phenomena. Additinally, the behaviour of such a complex nonlinear system as the earth's climate system may in general be chaotic.

However, models which include as internal variables as many interacting physical processes as possible to simulate observed phenomena are often too complicated to allow their results to be interpreted unambiguously and usually require a great deal of analysis and computer time in order to provide much understanding of the individual mechanisms and their dependence on each other. The interpretation of GCM results can unlikely be done successfully without the understanding derived from simpler models of individual processes. Schneider and Dickinson (1974) have argued that the primary role of the simpler models is in "making tentative estimates of the sensitivity of long-term conditions of the atmosphere-land-ocean-cryosphere system to changes to changes in various known thermodynamical and transport processes with a view identifying those of greatest importance". A climate modelling methodology that stresses intercomparison of models of differing complexity applied to the same problem can sharpen intuition and reduce misinterpretation of results. This step is clearly essential to the design and interpretation of more complicated and more realistic interactive models. The simplicity may lie in the reduced number of equations, in the reduced dimensionality of the problem, or in the restriction to a few processes. Thus, even with GCMs there are experiments run where a complex atmospheric GCM is coupled to a simple 'slab' ocean model, which is omitting ocean dynamics.

On the other hand, simplicity and questionable parameterizations may be the reason that energy balance models fail to give large responses. Perhaps if more physical processes were modelled, more feedbacks included, and more realism added, the models would become more sensitive. Simple climate models are useful mainly for examining global-scale questions.

# Chapter 2

# Climate (feedback) processes

A central question of climate studies is: What factors determine the Earth's climate? The climate system is a complex system consisting of the atmosphere, the lithosphere (solid land surface), the cryosphere (snow and ice), the hydrosphere (oceans and other bodies of water), and the biosphere (living ecosystems). A schematic overview about the various climate components is shown in figure 2.1, which is taken from IPCC-AR4.

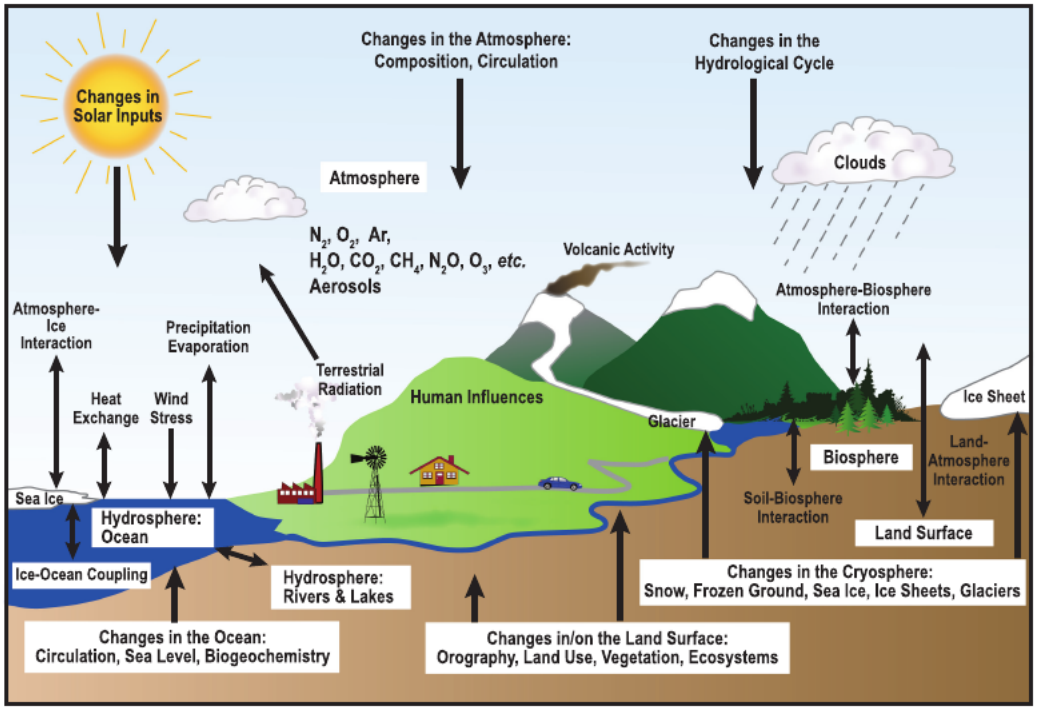


**fig.2.1** Schematic view of the components of the climate system, their processes and interactions. Source: IPCC-AR4.

The climate system evolves in time under the influence of its internal dynamics and due to changes in external forcings such as solar variations, volcanic eruptions, as well as anthropogenic influences. Under present conditions the earth's climate is changing due to natural

and anthropogenic forcings. The prediction of the amplitude and pattern of this change is the main focus of current research. One difficulty in predicting climate change is the large degree of cancellation that occurs between many of the climatic feedback mechanisms.

The fundamental determinants of the climate of the earth-atmosphere system are the input of solar radiation, the composition of the earth´s atmosphere, and the earth´s surface characteristics. The surface energy balance is

$$R \downarrow = LW \downarrow + Q_{sens} \uparrow + Q_{lat} \uparrow + G \tag{2.1}$$

where R is the absorbed solar insolation, LW is the longwave radiation, $Q_{sens}$ is the sensible heat flux, $Q_{lat}$ is the latent heat flux and G is the heat storage. For the climate to be constant in time the net addition of radiation to the surface, averaged over the globe for a long enough time, closely balances the fluxes of latent and sensible heat from the ocean surface into the atmosphere. If this is not the case, a change in climatic conditions is taken place. Variations in the radiation budget, however, will be followed by changes in the entire heat budget of the surface. Heat consumption by evapotranspiration and transfer of sensible heat to the atmosphere will be changed, and water vapour content, vertical lapse rate of temperature, and cloudiness will be changed in the same way. Without doubt, temperature is the one variable most generally regarded as being synonymous with climate. Corresponding to a surface energy balance an equilibrium temperature of the earth can be determined.The major part of the difference between the radiative equilibrium temperature (approximately -19°C) and the observed sea level average temperature (˜+15°C) is, of course, due to the so-called greenhouse effect of the atmosphere. In the following the physical factors affecting climate and climate change are described in more detail.

## 2.1 Radiation balance

The primary driver of the Earth's climate system is solar radiation. An overview over the Earth's radiation budget is given in figure 2.2. The amount of energy reaching the top of earth's atmosphere each second on a surface area of $1m^2$ facing the Sun during daytime is about 1370 Watts (IPCC-AR4), This value is termed 'solar constant'. The temporal mean value of received solar energy flux averaged over the entire planet is one-quarter of this ($342W/m^2$). On a global average about 30% of the sunlight reaching the top of the atmosphere is reflected back to space. A metric called 'albedo' is accounting for this reflection and varies with surface properties of the reflecting medium. Roughly two-thirds of the global average reflectivity is due to clouds and small particles in the atmosphere known as 'aerosols'. The remaining amount of the reflected solar energy is reflected by the surface, mainly by light surface types like snow, ice and deserts. The energy that is not reflected back to space (approximately 235 $W/m^2$) is absorbed by the earth's surface and atmosphere and is thus available for heat fluxes or temperature changes.

To balance the incoming energy, the earth itself must radiate, on average, the same amount of energy back to space. The earth does this by emitting outgoing longwave radiation. To emit 235 $W/m^2$, a surface would have to have a temperature of around -19°C, which is much colder than the conditions that actually exist at the earth's surface (15°C). The reason the Earth's surface is that warm is the presence of greenhouse gases within the atmosphere, which intercept and partially reemit the longwave radiation coming from the surface. This feature is known as the natural greenhouse effect. The most important greenhouse gases are water vapor ($H_2O_g$) and carbon dioxide ($CO_2$), followed by additional contributors such as methane ($CH_4$), nitrous oxide ($N_2O$), ozone ($O_3$) and chlorofluorocarbons (CFCs). Clouds have an effect similar to the GHGs; however, this effect is offset by their reflectivity, such that on global average, clouds tend to have a cooling effect on

climate. Local and temporary circumstances may yield a warming effect by clouds, as there is during cloudy nights or in polar regions.

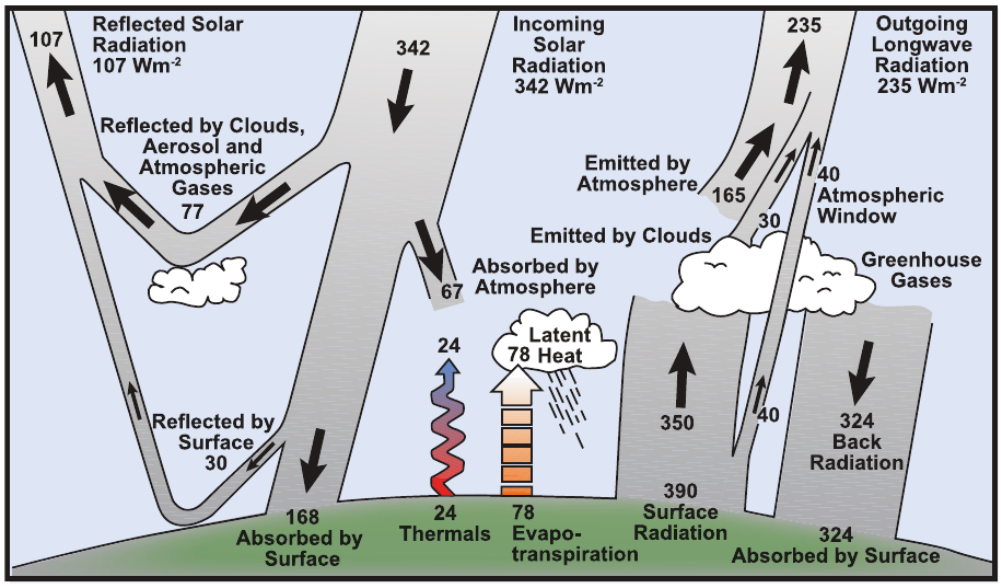


**fig.2.2** Estimate of the earth's annual and global mean energy balance. Over the long term, the amount of incoming solar radiation absorbed by the earth and atmosphere is balanced by the earth and atmsophere releasing the same amount of outgoing longwave radiation. About half of the incoming solar radiation is absorbed by the earth's surface. This energy is transferred to the atmosphere by warming the air in contact with the surface (thermals), by evapotranspiration and by longwave radiation that is absorbed by clouds and greenhouse gases. The atmosphere in turn radiates longwave energy back back to earth as well as out to space. Source: Kiehl and Trenberth (1997).

Because the earth is a sphere (neglecting geoidal deviations), the solar energy that arives at a given surface area is greater in the tropics than at higher latitudes, where sunlight strikes the atmosphere at a lower angle. The actual solar flux is the solar constant times a function S(x) which represents the mean annual distribution of radiation at each latitude. During a year the value of the solar constant varies by $\pm 3.5\%$ about its mean value. The function S(x) may be derived from celestial mechanics by using the tilt of the earth´s orbit with respect to the ecliptic plane, etc. (see Sellers, Physical Climatology, 1965; Cogley, 1979):

$$S_0 = \bar{S_0} * \left(1 + \left[\cos\left(\frac{2\pi}{365} * [JD - 21]\right) * 0.035\right]\right) \tag{2.2}$$

which is due to the eccentricity of the earth's orbit about the sun. The term JD accounts for the julian day of the year and JD=1 corresponds to January 1st.

$$S = S_0 * \sin\theta \tag{2.3}$$

where $S_0$ is the solar constant (1368 W/m$^2$) and $\theta$ the elevation angle (the complementary angle to the zenith angle Z: $\theta = \frac{\pi}{2} - Z$). The elevation angle $\theta$ is a function of latitude $\varphi$, solar declination $\delta$, and hour angle h:

$$\sin\theta = \sin\varphi \sin\delta + \cos\varphi \cos\delta \cos h \tag{2.4}$$

The declination varies within the interval from -23.5°C to 23.5°C and is given by:

$$\delta = 23.45 + \sin\left(360 * [284 + JD]/365\right) \tag{2.5}$$

The hour angle h is determined by the local time, whereby h=0 at noon. The difference between local time and UTC (Coordinated Universal Time) can be calculated from the longitude of each location:

$$\Delta t = -\lambda * \frac{24h}{360} \tag{2.6}$$

where $\lambda$ denotes the geographical longitude in degrees.

The amount of heat absorbed by the earth-atmosphere-system is the incident radiation flux times one minus the albedo of the earth-atmosphere system:

$$S_{abs} = S * (1 - \alpha) \tag{2.7}$$

The amount of longwave radiation emitted by the Earth's surface follows the Stefan-Boltzmann law, which is often referred to as the law of black-body radiation. However, the actual emitted energy also depends on the emissivity $\epsilon$ which only for perfectly 'black' bodies equals one:

$$LW = \epsilon * \sigma * T^4 \tag{2.8}$$

Hereby, $\sigma$ is the Stefan-Boltzmann constant $\left(5.6704 * 10^{-8} W m^{-2} K^{-4}\right)$and the emissivity $\epsilon$ is a dimensionless constant with a value depending on the emitting material. For simplicity one may assume that the earth as a whole emits radiation as a blackbody. The snow surface emissivity , for example, is $\epsilon$=0.970.

The almost-transparency of gases, such as CO2 and H2O, to solar radiation relative to their opaquness to IR radiation leads to the well-known greenhouse effect. The warm surface layer emits IR radiation, most of which is intercepted by optically active atmospheric gases, clouds, and particles. These constituents reemit radiation both up to space and back down to the surface, the downward radiation reducing the net loss of heat from the surface. Since the atmospheric emitters are colder than the surface, they emit proportionally less radiant energy. Consequently, the total outgoing IR radiation from the earth-atmosphere system is less the radiant energy emitted by the surface alone, and the effective radiation temperature of the earth is influenced more by the temperature of the colder atmospheric gases and cloud tops (which emit radiation roughly like a blackbody with the temperature of the atmosphere at the cloud tops) than by the warmer surface below. Variations in the CO2 concentration in the air change the long-wave downward radiation of the atmosphere and, thereby, the heat lost by radiation from the earth´s surface. The disturbed radiation budget will be compensated for, other things being equal, by an increased surface temperature.

By equating the energy fluxes and neglecting the greenhouse effect one can write the radiation balance equation for the surface:

$$\epsilon * \sigma * T^4 = S * (1 - \alpha) \tag{2.9}$$

In order to get more realistic results, one has to add a term representing the additional longwave radiation, which is emitted by the atmosphere and absorbed by the surface. This radiative flux can be derived in terms of surface temperature and other parameters characterizing the local greenhouse effect:

$$\epsilon * \sigma * T^4 - LW(T, c_{H_2O}, c_{CO_2}, ...) = S * (1 - \alpha) \tag{2.10}$$

If the albedo $\alpha$ is constant, there will be exatly one solution to this equation. However, If $\alpha$ has a steplike increase (at say -10°C) from one constant value (ice-covered earth) to

another constant value (ice-free earth), then there may be three solutions: ice-covered earth, near ice-free earth and intermediate solution. This is a major issue in climate dynamics. The radiation balance, in particular the functional relationship between albedo and temperature, seems to dominate the sensitivity of the "climate" to perturbation in energy inputs in energy balance models.

The optical properties of the atmosphere and the underlying surface determine the amount and location of the absorption of solar energy, the emission and absorption of infrared radiative energy, and consequently to a large extent the geographic distribution of heating of the atmosphere. The troposphere is essentially transparent to much of the solar radiation, which consequently is absorbed at the earth´s surface and either warms the surface or evaporates water, energy subsequently being released into the atmosphere in the form of latent heat. In the equatorial latitudes the absorbed solar energy generally exceeds the outgoing infrared energy, whereas in the polar latitudes the incoming absorbed solar energy is generally exceeded by the outgoing IR energy.

## 2.2 Water vapour feedback

According to IPCC-AR4 the water vapor feedback is the most important feedback enhancing climate sensitivity (positive feedback).The atmosphere is nearly opaque at wavelengths of strong water vapor absorption in the infrared. Tropospheric water vapor concentration is ultimately limited by saturation specific humidity, which strongly increases as temperature increases:

$$q_{sat} = 0.622 \bullet \frac{E}{p} = 3.75 \bullet 10^{-3} \bullet exp\left(\frac{17.08 \bullet t}{234.175 + t}\right) \tag{2.11}$$

with the saturation water vapor pressure E, the pressure p and the Celsius-temperature t.

Due to the dependence of saturation specific humidity on temperature, the average amount of water vapour in the atmosphere is assumed to increase as the tropospheric temperature increases. The assumption is based on the observation that the earth´s atmosphere, given sufficient time, appears to conserve a certain climatological distribution of relative humidity responding to the change of temperature (Manabe and Wetherald, 1967). The strength of absorption of longwave radiation by water vapor is roughly proportional to the logarithm of its concentration. Together with the near-exponential Causius-Clapeyron relation of the saturation specific humidity, this coupling results in an increased downward flux of longwave radiation and thus a decreasing effective radiation (loss) at the surface. In this way there will exist a self-intensifying or positive feedback effect in the heating process. Note that this is just a key positive feedback but not a forcing of climate change. Additionally, as with the emitted radiation, water vapour may also influence the absorbed solar radiative flux.

The atmospheric distribution of water vapor depends on several factors such as soilmoisture, evaporation, atmospheric temperature, vertical as well as horizontal processes, cloud formation processes and precipitation. Hence, almost all components of the hydrological cycle would have to be considered in order to make statements of atmospheric water vapor. A simple representation of the hydrological cycle is: mostly moisture is evaporated from the sea surface, where some precipitates out and the remainder is transported over land, where it also may be precipitated. In the real world the transport of atmospheric water vapor depends on the three-dimensional motions, which result in more or less effective horizontal moisture convergence and vertical mixing. Precipitation results from moisture convergence and from local evaporation from land, and runoff from land returns the moisture to the

sea. For the mean residence time of water vapor in the atmosphere one can consider a time period of 10 days.

Under climate change conditions the factors determining the atmospheric water vapor amount and distribution may be perturbed and thus initiate feedback mechanisms involved in the hydrological cycle. Because the moisture supply from the surface depends on evaporation and does not necessarily increase correspondingly with higher atmospheric temperatures, the soil moisture may be depleted. If the soil moisture falls below a critical point, evaporation is restricted, and the boundary layer gets drier. In time, a new balance is reached , in which potential increases in evaporation are restricted as a consequence of restricted moisture supply. Restricting evaporation means that the land surface warms more, because a higher temperature is needed to increase sensible heat loss and thermal radiation to compensate for the restricted evaporative cooling. This effect may further influence the observed land/sea contrast.

## 2.3 Ice albedo feedback

The albedo is the fraction of solar energy reflected back to space. Thus this surface property strongly affects the surface radiation balance. The strongest reflection of solar energy occurs in regions covered with snow or ice, whereas bare ground reflects only a minor portion. The cryosphere, which includes the large ice sheets of Greenland and Antarctica, continental (including tropical) glaciers, snow, sea ice, river and lake ice, permafrost and seasonally frozen ground, is an important component of the climate system. Next to low thermal conductivity, its large thermal inertia, its potential for affecting ocean circulation (through exchange of freshwater and heat) and atmospheric circulation (through topographic changes), its large potential for affecting sea level (through growth and melt of land ice), and its potential for affecting GHGs (through changes in permafrost), the cryosphere strongly affects the climate due to its high reflectivity (albedo) for solar radiation.

Due to the large contrast in albedo values a change from ice-covered to ice-free areas (or vice versa) may result in a large change in albedo and thus cause the so-called 'ice-albedo feedback'. Most notably in polar latitudes and middle latiudes during winter the extent and nature of ice and snow formation is the single most important climatological variable for determining surface albedo. Hence in these regions the ice-albedo feedback dominates the effects of climatic changes.

To a first approximation the surface albedo can be assumed to increase with temperature. This coupling leads to a strong positive feedback link between a change in surface temperature and a corresponding variation in albedo: colder temperatures cause more ice and snow and thus a higher albedo with a consequent reduction in absorbed solar energy, which in turn implies yet colder air temperatures in the glaciated region. This mechanism is termed 'ice-albedo feedback'. Therefore, ice cover is not only the consequence of cold climatic conditions, but also, to some extent, the cause of them. Such a positive feedback can multiply a comparatively small initial change in air temperature. The early models designed by Budyko (1968) and Sellers (1969, 1973) show the first-order importance of albedo-temperature coupling on climate stability.

The global mean solar radition reflected from the entire earth-atmosphere system back to space by clouds, aerosols, and surface conditions is given by a planetary albedo of approximately 0.30. On a global average the albedo for the cloudless part of the earth-atmosphere system is about 0.14 (according to London and Sasamori, 1971) and for the cloud-covered part its value is about 0.5. In accordance to an average cloud cover of approximately 50% this gives the stated mean albedo.

To a lowest approximation one can distinguish between the albedo of the oceans, that of

dry land surfaces, and that of snow-ice surfaces. More realistically, the surface albedo varies strongly within these catagories as can be seen from the following table (after Sellers, 1965):

| surface type | reflectivity (%) |
|---|---|
| water, plane surface | 2.4 |
| water, at equator | 6.0 |
| water, diffuse solar radiation | 17 |
| water, 60° latitude in winter | 21 |
| snow, fresh fallen | 75-95 |
| sea ice | 30-40 |
| soil, dark | 5-15 |
| soil, dry light sand | 25-45 |
| forest, coniferous | 5-15 |
| crops | 15-25 |

The albedo of the ocean shows a strong dependence on the sun's mean elevation and the corresponding angle of incidence of direct solar radiation. It is usual to average this dependence in some way over time, and to set down the albedo as a function of latitude. Estimated from Raschke et al., 1973 this relation is:

$$\alpha_{ocean}(\varphi) = 0.33 - 0.125 * \cos(2\varphi) + 0.007 * \exp(\varphi^2) \tag{2.12}$$

The dependence of the sea surface albedo on solar zenith angle is such that the albedo of the sea surface increases with increased solar zenith angle. Thus increasing the solar zenith angle reduces the effect of changes in the surface albedo on the earth-atmosphere system albedo and should be accounted for since ice-albedo-temperature feedback is most active in high latitudes – precisely the regions of high solar zenith angle. As a result the change in albedo as the surface changes from ice-free to ice-covered conditions will be large at low latitudes but small at high latitudes, where the ice-cover changes take place. Allowing for the zenith angle-dependent reflectivities referred to by Lian and Cess (1977) finds that the change in albedo at the ice line is reduced to 0.15.

Minor changes in ocean albedo are controlled by variation in water turbidity, wave height, and the ratio of diffuse and total radiation. Another fact is that water albedo is virtually constant under diffuse radiation, at a value between 6 and 10%. Diffuse radiation should therefore reduce the marked dependence of the ocean albedo on elevation angle, raising low values and reducing high ones.

Under climate change conditions the ice and snow cover on the earth's surface may change considerably. Since the massive continental ice caps of Antarctica and Greenland are generally believed to vary on a time scale of millennia they may be specified as given external conditions for model calculations on shorter time scales. However, in the real world they certainly will change and cause alterations in surface albedo, freshwater fluxes and other climatic parameters. On the other hand, land and ocean covered with ice or snow are strongly affected by climate change. New sea ice develops in high latitudes during the wintertime by cooling of the ocean surface to freezing temperatures [$T_{ice}$=-2°C]. Temperatures above this value will therefore result in melting processes. The formation of ice and snow on land depends on surface temperature, precipitation, and other factors that determine the surface energy budget and hydrological cycle.

Although according to IPCC-AR4 the principle of the albedo feedback is simple, a quantitative understanding of the effect is still far from complete. For instance, it is not clear whether this mechanism is the main reason for the high-latitude amplification of the warming signal.

## 2.4 Surface heat fluxes

There are two different types of heat fluxes, that complete the energy balance at the surface, which has sofar only consisted of the radiation balance: the sensible ($Q_{Sens}$) and the latent heat flux ($Q_{lat}$). Both will be described in the following.

Sensible and latent heat are transferred from the surface to the atmosphere primarily by small-scale turbulent motions. Since these processes are difficult to measure several parameterizations have been developed for the boundary layer transports: the vertical fluxes of sensible and latent heat through the planetary boundary layer averaged over time and space can be expressed by the bulk transfer equations. The flux within the constant flux layer is usually related to a non-dimensional 'drag coefficient' $C_D$ times the quantity being transported times the velocity of the atmosphere, all being evaluated at some reference level (typically 10m) within the constant stress layer (taken from Kent and Taylor, 1995):

$$Q_{sens} = \rho * c_p * (T_0 - T) * C_D * |\vec{v}| \tag{2.13}$$

$$Q_{lat} = \rho * L * (q_0 - q) * C_D * |\vec{v}| \tag{2.14}$$

with the air density $\rho$, the specific heat capacity $c_p$ of air, the air temperature $T_0$, the surface temperature T, the absolute velocity $|\vec{v}|$, the latent heat of evaporation L, the saturation specific humidity $q_0$ and the atmospheric specific humidity q. The drag coefficient $C_D$ at 10m has been determined experimentally to be of the order of $10^{-3}$, although there may be some dependence on velocity and on the nature of the surface (Hicks, 1972). For natural open ground average values for the bulk transfer coefficient for latent heat are 1.18-1.30*$10^{-3}$ according to Kondo (1975). Over a snow surface its value is estimated at $C_E$=2.1*$10^{-3}$ by Kondo and Yamazawa (1986).

As can be seen in figure 2.2, the latent heat flux is an important contributor to the global energy balance. Energy is required to evaporate water from the sea or land surface, and this energy (latent heat), is released when water vapor condenses during cloud formation in the atmosphere. Latent heat release is also a primary driver of the atmospheric circulation. For the earth as a whole, Sellers (1965, p.104) asserts that evaporation accounts for 82% of the net radiation and turbulent heat exchange for 18%, and thus the main method by which the radiative heat surplus of the earth´s surface is dissipated and transferred vertically to the atmosphere is by evaporation of water. The latent heating of the atmosphere varies primarily with latitude but also has important longitudinal gradients as a consequence of the distribution of land and ocean surfaces. Latent heat originates primarily in the subtropics (15°-35°N, 15°-35°S) where annual evaporation exceeds annual precipitation.

The latent heat flux to the atmosphere is always positive and increases with increasing wind speed. It is found over land that the relative magnitudes of upward fluxes of sensible and latent heat are quite sensitive to soil moisture, the ratio $\frac{Q_{sens}}{Q_{lat}}$ ranging from 0.1 over a water surface to about 0.5 over vegetated areas to 10 or greater over dry or desert areas (Sellers 1965). The ratio B=$\frac{Q_{sens}}{Q_{lat}}$ is sometimes referred to as Bowen ratio. Vegetation covers a major part of the land surface and promotes efficient energy exchange as the result of 1) active turbulence caused by its large roughness, 2) a multilayer energy exchange with its environment, and 3) the transpiration from its leaf surfaces. Although the energy exchange at a vegetated surface takes place in the multilayers within the canopy, it is often assumed that the canopy and ground can be regarded as a single plane surface.

According to Kondo et al. (1990) surface evaporation is one of the main processes in the air-land energy exchange. The evaporation rate is controlled by atmospheric conditions, surface soil wetness, and moisture transport in the soil layer affected by the soil moisture. The evaporation process is usually parameterized by the so-called "surface moisture

availability" ($\beta$), such that the following definition is attained:

$$Q_{lat} = \beta * \rho * L * (q_0 - q) * C_D * |\vec{v}| \tag{2.15}$$

It is generally assumed that a given soil type will hold a certain amount of water that is accessible to evaporation (or transpiration). Thus latent heat flux values for $\beta$=1 are greater than for $\beta$=0.

Obviously, the latent heat flux is associated with a corresponding flux of water vapor from the ground into the atmosphere. The latent heat flux can be written as:

$$Q_{lat} = L * E \tag{2.16}$$

where L is the latent heat of evaporation and E is the water vapor flux.

The major source region for both atmospheric and oceanic sensible heat lies in the tropics between 20°N and 20°S. In contrast to the transfer coefficient of latent heat flux, that of sensible heat flux does not depend markedly on velocity or surface roughness. Thus for practical purpose, the average value of 1.15-1.26*$10^{-3}$ should be sufficiently accurate (Kondo, 1975). However, sometimes higher values are mentioned in the literature.

## 2.5 Clouds

Clearly, cloud amount feedbacks could greatly influence the sensitivity of the climate. However, the effect of changes in cloudiness on surface net heating depends upon the local values of the cloud amounts, heights, and albedos, the albedo of the surface, the average solar zenith angle, and the local vertical distribution of temperature and optically active constituents. This complex system results in feedback mechanisms that may either amplify or cancel each other to some extent. The present-day global average value of cloud cover is 50%, but the distribution of clouds within the atmosphere is horizontally as well as vertical heterogeneous.

Clouds may strongly affect the radiation balance of the surface. Of the solar radiation reflected by the earth, clouds reflect between 70 and 80% on a global average. Albedos of clouds due to droplets are given by Schneider and Dickinson (1974):

| cloud level | high | middle | low |
|---|---|---|---|
| albedo | 0.21 | 0.48 | 0.69 |

There are several ways that clouds can produce feedback mechanisms. All of the models contributing to the current IPCC report (2007) are consistent as to the sign of the change in cloud amount (i.e., cloud cover decreases for climate warming); although the magnitude of this change varies significantly from model to model. For example, if global cloud amount decreases because of climate warming, then this decrease reduces the infrared greenhouse effect due to clouds. Thus as the earth warms, it is able to emit infrared radiation more efficiently, moderating the global warming and so acting as a negative climate feedback mechanism. But there is a related positive feedback: the solar radiation absorbed by the surface-atmosphere system increases because the diminished cloud amount causes a reduction of reflected solar radiation by the atmosphere. Thus, there are two competing opposite effects on the global radiation balance from an increase in the amount of global cloud cover. The change in cloud cover, however, provides only limited information with regard to interpreting cloud feedback. The situation is further complicated by climate-induced changes in both cloud vertical structure and cloud optical properties, which result in additional infrared and solar feedback (Cess and Potter, 1988).

Another possible change in cloudiness is a variation in the average or effective height of the cloud tops. Since on average higher cloud tops are colder than the lower ones, and thus emit proportionately less blackbody radiation than the lower clouds, an increase of the effective height of the cloud tops reduces the upward flux of the IR radiation escaping from the earth-atmosphere system to space. In addition, the effect of variations in cloud amount on the local radiation balance will depend upon the local average solar zenith angle. This dependence is particularly important for large zenith angles typical of polar regions. Generally speaking, the larger the cloud amount, the colder is the equilibrium temperature of the earth´s surface, though this tendency decreases with increasing could height and does not always hold for cirrus and near polar regions, where the albedo of the cloudy areas can be comparable to (or even smaller than) the albedo of the snow-covered cloudless areas, and where, especially in the winter season, the amount of incoming solar radiation at high latitudes is much less than the global average value of insolation.

As an overall result a change in cloudiness does not necessarily imply that a change in the surface energy balance must accompany the change in cloudiness. If both the amount and height of the clouds change in such a way that the amount of absorbed solar radiation still equals the emitted longwave radiation, then no change in the radiation balance need occur and the surface temperature remains unchanged.

Clouds are an important component of the hydrological cycle and play a significant role for the atmospheric circulation since cloud formation is associated with latent heat release in the atmosphere. Associated with actual climatic change variations in the equator-to-pole temperature gradient, wich is a primary driving force of the atmospheric general circulation, may alter the cloud distribution pattern. This effect, by itself, may produce a cloud feedback component.

In the current climate, clouds exert a cooling effect on climate. In response to global warming, the cooling effect of clouds on climate might be enhanced or weakened, thereby producing a radiative feedback to climate warming. For their $CO_2$ doubling simulations, Wetherald and Manabe (1988) found that cloud feedback amplified global warming by the factor 1.3. The models within the IPCC AR4 all predict a positive cloud feedback but strongly disagree on its amplitude (see figure 8.14 in the report). Nevertheless, according to IPCC-AR4 cloud feedbacks still remain the largest source of uncertainty.

## 2.6 Horizontal advection

Atmospheric and oceanic dynamics are associated with horizontal and vertical heat transports that are an important contributor to the energy balance. The incoming absorbed radiation at one location is not exactly balanced by infrared outgoing radiation and heat fluxes because of the transport of heat parallel to the earth´s surface. Hence changes in the energy balance at one location may affect that of the near surrounding as well as remote regions. Thus, for example, land temperatures are tightly coupled, through atmospheric transport, to SSTs. The transport of heat can influence the sensitivity of the climate system, for example, through its impact on the albedo-temperature feedback.

The differential heating of the globe, coupled with the rotation of the earth, is the ultimate driving force behind the winds and ocean currents, whereas the energy-transporting ocean currents are mainly driven by wind-stress (Ekman transport). These winds and currents, which make up the geophysical fluid system concerning the earth surface, regulate the distribution of temperature, cloudiness, and precipitation over the globe. In general, (sensible) heat and water vapour (latent heat) are transported through atmospheric mean and transitory (eddy) motions. On the average, heat is carried from warm equatorial areas to cool higher latitudes by an amount proportional to the gradient of the temperature. The

one exception is the latent heat flux, which, as a result of a strong Hadley circulation, is directed equatorward between 20°N and 20°S. This way the atmospheric advection is adjusting with the radiative processes through transport of heat from areas of positive radiation balance to areas of negative balance. Latent heat is carried by the water vapour evaporated at the earth´s surface. In the presence of suitable nuclei (particles) and saturation the water may condense into drops, thereby releasing the latent heat that was needed originally to change it from liquid to vapour. The atmospheric circulation systems become more vigorous with increasing north-south temperature gradients applied at the lower boundary, so that large-scale transient eddies (storm systems), which transport additional heat poleward, provide 'negative feedback', lessening the increase of the equator-to-pole temperature difference. The oceans carry the remainder of total heat flowing poleward. A large portion of the oceanic heat transport takes place in the mixed layer Ekman drift currents, where temperatures depend on atmospheric influences. It is generally believed, however, that much of the global scale net horizontal transport of energy by the oceans occurs below the level to which the seasonal thermocline penetrates.

Vertical transfer of heat is often parameterized by eddy mixing and large-scale convection. The time scale for changing the temperature of the underlying layers below the mixed layer is approximately one decade, so that for studying fluctuations on the time scale of a year it may be sufficient to take the temperature of the underlying layers to be given.

## 2.7 Thermal inertia

Nearly all processes determining the earth's climate vary among the different locations on the surface. The surface characteristics determine to what extent local feedback mechanisms may alter the energy balance.

The top layers of the ocean are completely mixed by the turbulence associated with generation of surface waves. In winter this mixed region is deepened significantly by downward convection of dense water formed by cooling and ice formation at the surface. The net heat input is very quickly distributed in the vertical direction throughout the mixed layer depth. The temperature of the mixed layer as a whole adjusts to this net heating (or cooling) and entrainment of fluid from below by increasing (or decreasing) until thermal balance is achieved. At the base of the mixed layer the temperature drops (or sometimes rises) to its value at the top of the stably stratified underlying water. The seasonally varying interface between the bottom and the underlying stratified region is known as the 'seasonal thermocline'. Depending on the depth of the mixed layer, the ocean surface temperature responds rather fast or slowly to changes in the energy balance. This effect is represented by the specific heat capacity, which is most important for the seasonal cycle, since it is a measure for the thermal inertia of a system. The higher the heat capacity the longer the time the system needs to return from a perturbation back to equilibrium. Thus land surfaces will have large amplitude and short phase lag due to a smaller specific heat capacity, while ocean surfaces will have small amplitude and nearly quarter-cycle phase lag.

But even within the ocean regions this heat capacity of the mixed layer may vary seasonally as well as spatially due to different mixed layer depths. The variation in depth of the seasonal thermocline is primarily a function of the amplitude of the seasonal cycle of incoming solar energy. Hence there is a rather permanent vertical structure in tropical latitudes, where the seasonal variation in solar input is relatively small, and an increasing amount of seasonal variation in the structure of the upper layers of the ocean with latitude, since the amplitude of the seasonal cycle of solar input increases with latitude. There are exceptions, for example due to the influence of clouds and the mixing of heat to greater depths (presumably due to stronger winds).

For sea ice as well as land ice the value of heat capacity is intermediate between that of land and ocean. It should also simulate the effects of melt water, etc.. It is found to be about 9 times that of land. For the heat capacicty of the atmosphere one can consider a vertically integrated one-layer atmosphere (up to about 10km).

## 2.8 Changes in orbital parameters

Besides internal processes the changes of the external boundary conditions may alter the earth's climate. Among those external influences are the changes in orbital parameters. Over periods of $10^4$-$10^5$ years the earth´s orbit about the sun changes with respect to its eccentricity (period of approx. $10^5$ years), axial tilt (41000 yr) and its precession (approx. 26000 yr).

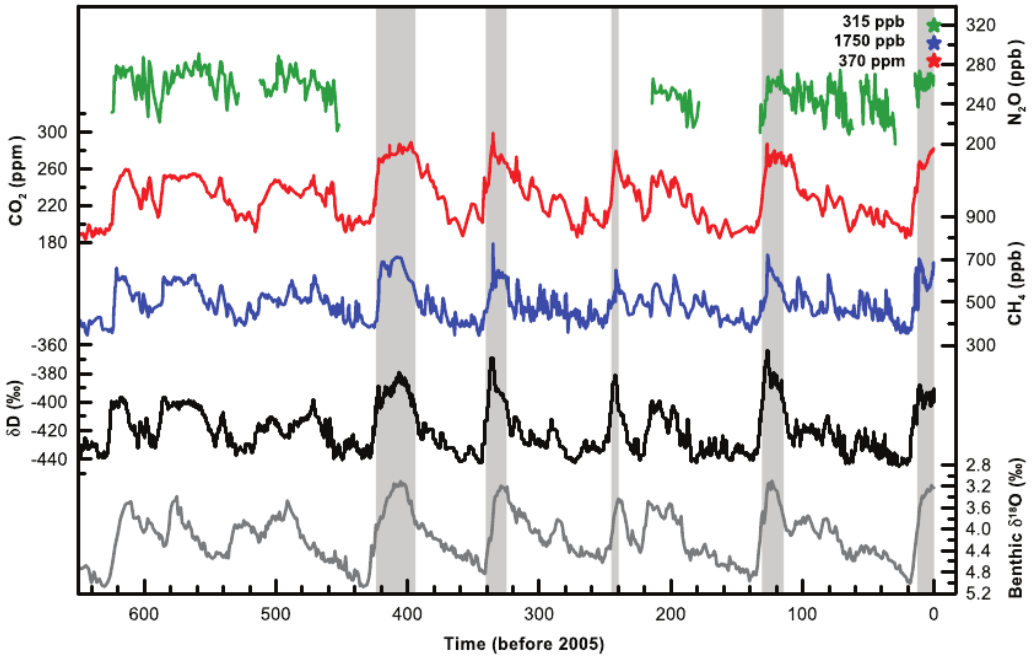


**fig.2.3** Variations of deuterium ($\delta$D; black), a proxy for local temperature, and the atmospheric concentrations of the greenhouse gases $CO_2$ (red), $CH_4$ (blue), and nitrous oxide ($N_2O$; green) derived from air trapped within ice cores from Antarctica and from recent atmospheric measurements (Petit et al., 1999; Indermühle et al., 2000; EPICA community members, 2004; Spahni et al., 2005; Siegenthaler et al., 2005a,b). The shading indicates the last interglacial warm periods. Interglacial periods also existed prior to 450 ka, but these were apparently colder than the typical interglacials of the latest Quaternary. The length of the current interglacial is not unusual in the context of the last 650 kyr. The stack of 57 globally distributed benthic $\delta$18O marine records (dark grey), a proxy for global ice volume fluctuations (Lisiecki and Raymo, 2005), is displayed for comparison with the ice core data. Downward trends in the benthic $\delta$18O curve reflect increasing ice volumes on land. Note that the shaded vertical bars are based on the ice core age model (EPICA community members, 2004), and that the marine record is plotted on its original time scale based on tuning to the orbital parameters (Lisiecki and Raymo, 2005). The stars and labels indicate atmospheric concentrations at year 2000.

Milankovitch (1941), among others, argued that these changes cause variations in the amount and distribution of solar radiation received by the earth, thereby influencing the climate. Milankovitch suggested that the orbital changes force the advance and retreat of glaciers. Indeed, evidence that the climate is so forced has been found in geological records (deep-sea and ice cores). In figure 2.3 time series of several parameters describing the earth's climate are shown. The first deep ice cores from Vostok in Antarctica revealed a highly correlated evolution of temperature changes and atmsopheric composition on millennial time scales.

## 2.9 Other processes

The list of physical, chemical and other processes governing the climate system can be extended further, inlcuding more more and more details, but this is not the aim of this work. Nevertheless there are some other processes worth to mention.

The solar radiation emitted from the sun varies due to changes in the sun's activity. At the maximum of the 11-year solar activity cycle, when sunspots are at their maximum, the total solar irradiance is larger by about 1% than at the minimum. Thus, a corresponding cycle in solar forcing is influencing the earth's climate. Calculations with three-dimensional models (Wetherald and Manabe, 1975; Cubasch et al., 1997; Lean and Rind, 1998; Cubasch and Voss, 2000) suggest that the changes in solar radiation could cause surface temperature changes of the order of a few tenths of a degree Celsius.

Further influences on climate result from the hydrological cycle such as: snow accumulation rates over glaciers, snowmelting processes, heat transfer by precipitation and so on. There are several processes usually regarded as being second order globally: dissipation of mechanical energy by winds, waves and tides; photosynthesis; oxidation of biological material (which can be very large locally); fires, volcanic aerosols (cooling effect), and heat released by man´s activities.

A potentially more important process for further climate changes is the change in dynamics of the atmospheric circulation and oceanic currents. As discussed by Folland et al. (2001), recent warming has been greatest over the mid-latitude Northern Hemisphere continents in winter, and a component of the signal may be explained by the sharp increase in the positive phase of the North Atlantic Oscillation (NAO).

Another process that may influence the greenhouse gas concentration thus lead to a positive feedback mechanism is the permafrost-climate feedback, which plays an important role, not only for polar regions. As permafrost thaws due to a warmer climate, greenhouse gases such as $CO_2$ and methane trapped in the frozen soil are released to the atmosphere. Thus, atmospheric temperature is likely to increase and hence causing a further thawing of the permafrost. The permafrost and seasonally thawed soil layers at high latitudes contain about one-quarter of the global total amount of soil carbon. Because global warming signals are amplified in high-latitude regions, the potential for permafrost thawing and consequent greenhouse gas releases is thus large.

One of the feedback mechanisms that was included into many current climate models is the carbon feedback mechanism. If all the $CO_2$ produced by man remained in the atmosphere, its concentration would grow rapidly. However, because of the constant exchange of $CO_2$ between the atmosphere and the ocean (which can absorb a great amount of carbon dioxide), only part of anthropogenic $CO_2$ remains in the atmosphere. Warming reduces terrestrial and ocean uptake of atmospheric $CO_2$, increasing the fraction of anthropogenic emissions remaining in the atmosphere. This positive carbon cycle feedback leads to larger atmospheric $CO_2$ increases and greater climate change for a given emissions scenario.

However, many of these processes are not fully understood and require further research.

Thus their implementation into climate change considerations increases the uncertainties in the results.

## 2.10 Resulting feedback mechanisms

In order to summarize the complex feedback mechanisms that may play a role in determining the amplitude and pattern of climate change, there will follow a listing and schematical represantation of the main features.

**1)** Temperature-radiation feedback:

- thermal radiation depends on absolute temperature
- increased thermal radiation will act to restore temperature back to its equilibrium value
- limits stabelizes the temperature response to changes in the energy input (negative feedback)

**2)** water vapour-greenhouse feedback (positive)

- the atmosphere is believed to maintain a somewhat uniform distribution of relative humidity over a large range of lower atmospheric temperatures (Möller, 1963) even though the absolute amount of water vapour in the air varies strongly with atmospheric temperature.
- absolute amount of water vapour in the atmosphere determines to a large extent the opacity of the lower atmosphere to IR radiation
- increased atmospheric temperature at constant relative humidity leads to increased trapping of thermal radiation ('greenhouse effect'), which gives rise to further increases in temperature of the lower atmosphere

**3)** snow and ice cover albedo – temperature feedback

- high reflectivity of snow and ice as compared to that of water and land surfaces is a dominant factor in the climate of polar regions
- lower temperature would increase the albedo, causing a decrease in the amount of solar energy absorbed by the earth-atmosphere system, and would thereby lower the temperature further (positive feedback)
- hydrological processes should also be included in this feedback loop, since ice and snow are merely the solid phase of water. Thus the strong positive link between the extent of snow and ice cover and the local temperature assumed in the preceding discussion will be effective only insofar as there is an appropriate amount of precipitation, f.e., to build up continental glaciers or snow cover on sea ice (Kellogg, 1974).

**4)** cloudiness-surface temperature coupling

- most clouds are both excellent absorbers of IR radiation and good reflectors of solar energy
- because both solar energy absorption and planetary IR emission decrease with increasing cloud cover amount, we must consider quantitatively the geographic distribution of cloud amounts, cloud heights, and cloud optical properties in order to calculate the net effect of changes in cloud parameters on the surface radiation balance
- the direction of possible climate feedback between cloudiness and surface temperature is not yet clear

**5)** radiative-dynamic coupling

- changes in the radiation balance will result in a redistribution of this heat by atmospheric motions, which may either offset or accelerate any climate changes linked initially to the original perturbation in radiation balance

**6)** ocean-atmosphere coupling

- in addition to the obvious role of the oceans in providing water for the hydrological cycle the dynamic coupling of atmospheric winds and temperatures with ocean circulation SSTs plays a major role in determining our climate.
- the vast thermal capacity of the oceans limits the extremes of seasonal climate that would otherwise be experienced in the middle and polar latitudes were it not for the presence of the oceans. This effect increases the response time of the surface temperature to changes in external energy input.

From this perspective a key question arises: Is it possible to simulate the surface warming pattern with a simple model for global warming that only realizes a finite number of these feedback processes?

# Chapter 3

# Climate change

In the recent Assessment Report of the Intergovernmental Panel on Climate Change (IPCC-AR4) climate change is defined as follows:

> Climate change in IPCC usage refers to change in the state of the climate that can be identified (e.g. using statistical tests) by changes in the mean and/or the variability of its properties, and that persists for an extended period, typically decades or longer. It refers to any change in climate over time, whether due to natural variability or as a result of human activity.

Thanks to numerous and long enough observational records of climatic parameters, the recent changes in climate can be visualized (see figure 3.1). The global average temperature has increased during the last 150 years and from the global record a 100-year linear trend (1906-2005) was estimated to 0.74K. For the last 50 years (1956-2005) the linear warming trend is even twice as high, with a value of 0.13 K/decade. This warming was accompanied by a global sea level rise and widespread melting of snow and ice on the northern hemisphere. The letter is linked to the amplified warming trend in polar regions. Thus the Arctic sea ice extent has shrunk, whilst Antarctic sea ice extent shows interannual variability but no statistically significant average multi-decadal trend, consistent with the weak temperature rise over the Antarctic continent. On the remaining continents mountain glaciers and snow cover have declined in both hemispheres.

Additionally there have been observed trends in other climatological parameters, such as precipitation, the variability of extreme weather events and atmospheric and oceanic local circulation patterns. Over the last hundred years, precipitation increased significantly in eastern parts of North and South America, northern Europe and northern and central Asia whereas precipitation declined in the Sahel, the Mediterranean, southern Africa and parts of southern Asia. Thus also the soilmoisture will be affected.

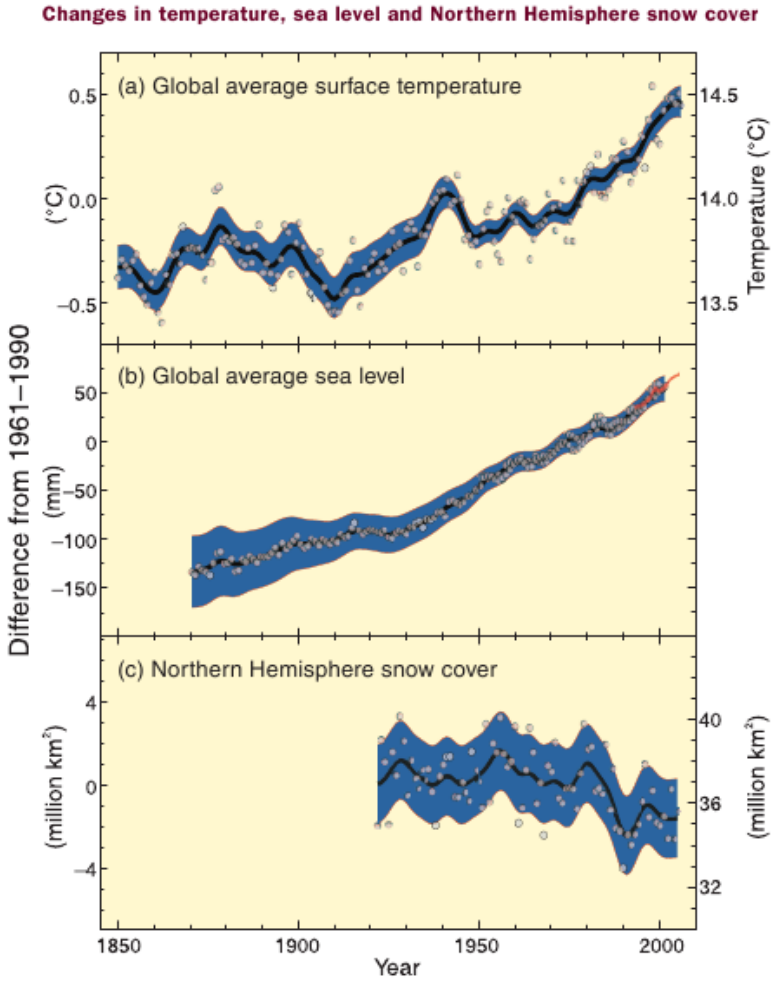


**fig.3.1** Observed changes in (a) global average surface temperature; (b) global average sea level from tide gauge (blue) and satellite (red) data; and (c) Northern Hemisphere snow cover for March-April. All diefferences are relative to corresponding averages for the period 1961-1990. Smoothed curves represent decadal averaged values while circles show yearly values. The shaded areas are the uncertainty intervals estimated from a comprehensive analysis of known uncertainties (a and b) and from the time series (c). Source: IPCC-AR4

Now the question arises about the reasons for this change in the earth's climate. When climate is viewed as a time-mean state, changes in the system on time scales that are long in comparison with a given interval may arise from either long-period external influences or other internal changes. Thus climate change may result from either naturally occurring processe or changes in external forcings, the letter including anthropogenic influences. It is indeed possible for climate change to be inferred from natural time variations of the entire climate system without the presence of any external influence. However, the currently observed changes in the earth's climate are at least partially induced by anthropogenic influences. Fluctuations on a shorter timescale are then regarded as noise.

Changes in the external system, either naturally occurring or man induced could be, for example, fluctuations in solar emission, influence of variations in the earth´s orbital pa-

rameters, changes in atmospheric carbon dioxide, changes in atmospheric dust and changes in the character of the land surface (e.g., albedo).

As the time scale of climate change is expanded, the internal system will ultimately include all parts of the oceans, snow and ice fields, and possibly even parts of the biosphere as well as the atmosphere. The external system will then reduce to those conditions truly uncoupled from the internal system: for example, the ocean and land topography and the distribution of incoming solar radiation.

## 3.1 Natural climate variability

Natural forcings causing climate change arise due to solar changes and explosive volcanic eruptions. Ths solar energy follows an 11-year cycle (see figure 3.2) and may also undergo non-cyclic trends due to changes in solar activity and celestial parameters. While directly heating the climate system the solar energy can also affect the atmospheric abundance of some GHGs, such as stratospheric ozone. Explosive volcanic eruptions, such as those of El Chichón in 1982 and Mt. Pinatubo in 1991, can create a short-lived (2 to 3 years) negative forcing through the temporary increases in sulphate aerosol in the stratosphere, which are formed as a result of oxidation of the sulphur gases emitted by these eruptions. Minor radiative perturbations result from volcanic ash particulates, but these sediment out of the stratosphere fairly rapid due to gravity.

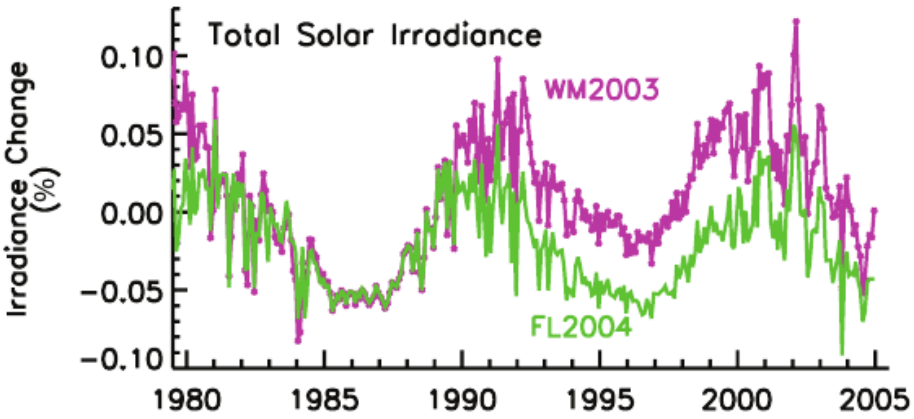


**fig.3.2** Percentage change in monthly values of the total solar irradiance composites of Willson and Mordvinov (2003, WM2003, violet symbols and line) and Fröhlich and Lean (2004, FL2004, green solid line). (taken from IPCC AR4, 2.7)

However, there is a theory about climate change which is solely due to internal variability of the system. Already Lorenz (1968, 1970) stated: 'Might not some scales of climate change be nothing more than natural fluctuations arising solely from the complex nonlinear interactions between land, oceans, atmosphere, and polar ice? These components of the climate system have the capacity to store or to release vast amounts of energy on time scales ranging from days to centuries. These fluctuations could be inherent in the complex, natural climatic system and might not necessarily be a result of changes in the external environment (such as CO2 amount or variations in solar input). Furthermore, it is possible that natural fluctuations could occur an time scales very long with respect to the observational data gathering periods of man, and thus appear to us as distinct stages, the explanation of which might tempt us to look for external causes'.

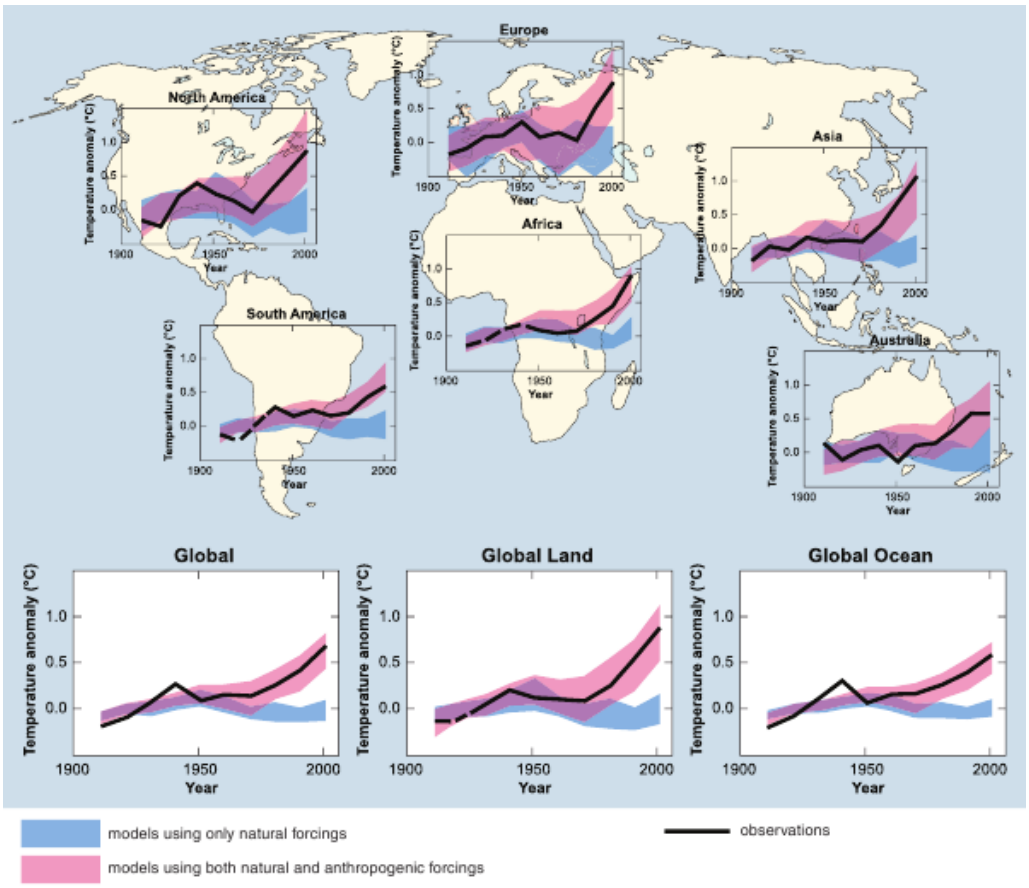


**fig.3.3** Comparison of observed continental- and global-scale changes in surface temperature with results simulated by climate models using either natural or both natural and anthropogenic forcings. Decadal averages of observations are shown for the period 1906-2005 (black line) plotted against the centre of the decade and relative to the corresponding average for the 1901-1950. Lines are dashed where spatial coverage is less than 50%. Blue shaded bands show the 5 to 95% range for 19 simulations from five climate models using only the natural forcings due to soalr activity and volcanoes. Red shaded bands show the 5to 95% range for 58 simulations from 14 climate models using both natural and anthropogenic forcings. (taken from IPCC-AR4)

Nevertheless, according to IPCC-AR4 the observed widespread warming of the atmosphere and ocean, together with ice mass loss, support the conclusion that it is extremely unlikely that the global climate change of the past 50 years can be explained without external forcing and very likely that it is not due to known natural causes alone. As is shown in figure 3.3 from the IPCC-AR4, climate models that are only driven by natural forcing fail to reproduce the obeserved surface warming trends. In fact, in today's atmosphere, the radiative forcing from human activities is much more important for current and future climate change than the estimated radiative forcing from changes in natural processes.

## 3.2 Global Warming

The atmospheric concentrations of long-lived greenhouse gases (GHGs) dominated the radiative forcing of the earth's climate system (IPCC-AR4). Should the amount of an IR-absorbing gas in the troposphere be increased, it would then intercept a larger fraction of the IR energy coming upward from the warmer layers near the surface (greenhouse effect). For the balance between IR emission to space and solar flux absorption by the earth-atmosphere system to be maintained, on the assumption that the planetary albedo remains unchanged, the surface temperature must rise. With increased $CO_2$ the tropospheric temperature change is dominated by the increased trapping of upward thermal radiation from the ground, whereas the stratospheric temperature change is dominated by $CO_2$ IR cooling to space.

The global GHG emissions due to human activities have grown since pre-industrial times, as can be seen in figure 3.4 which has been taken from the IPCC-AR4. Emissions are given in $CO_2$-equivalents ($CO_2$-eq.). This unit takes care of the different radiative forcing potentials and lifetimes of the various greenhouse gases. The $CO_2$-eq. is the amount of $CO_2$ emission that would cause the same time-integrated radiative forcing, over a given time horizon, as an emitted amount of a long-lived GHG or a mixture of GHGs. Human activities cause emissions of mainly four different long-lived GHGs: carbon dioxide, methane, nitrous oxide ($N_2O$) and halocarbons, the letter being substances containing fluorine, chlorine or bromine. Minor contributions affect the concentrations of sulphur hexafluoride ($SF_6$). As long as the emissions of those GHGs exceed the removal rates their atmospheric concentrations will increase. Thus, due to anthropogenic emissions the GHG concentrations in the earth's atmospere have increased in the past more than a hundred years and are now far above pre-industrial levels. According to the IPCC-AR4, most of the observed increase in global average temperature since the mid-20th century is *very likely* due to the observed increase in anthropogenic GHG concentrations. In the following, several GHGs are considered.

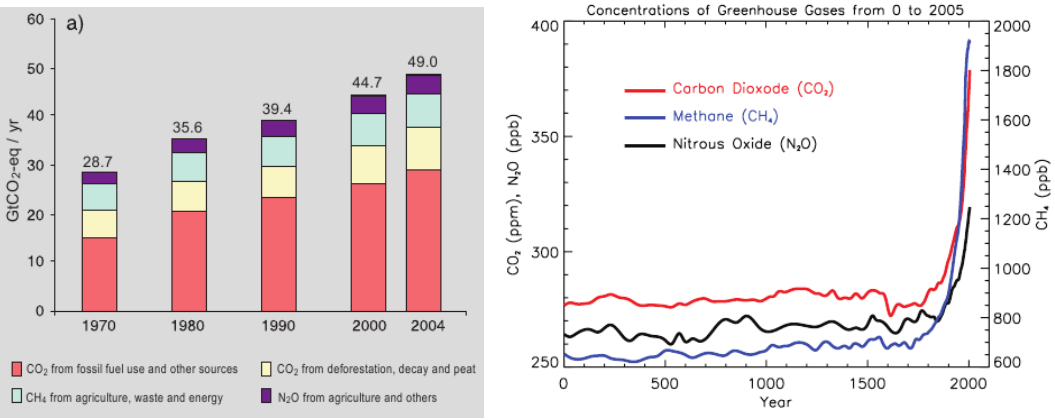


**fig.3.4** (left) Global annual emissions of anthropogenic GHGs from 1970 to 2004. (right) Atmospheric concentrations of important long-lived GHGs over the last 2000 years. Increases since about 1750 are attributed to human activities in the industrial era. Concentration units are parts per million (ppm) or parts per billion (ppb), indicating the number of molecules of the GHG per million or billion air molecules, respectively, in an atmospheric sample. (taken from IPCC AR4, 2.2)

Whereas water vapor dominates the natural greenhouse effect, carbon dioxide is the most important anthropogenic greenhouse gas. As shown in figure 3.4, the $CO_2$ concentration

has tremendously increased above its pre-industrial (before 1750) value of about 275 to 285 ppm over the last 250 years, reaching a concentration of approximately 379ppm in 2005. The absolute rate of growth is still increasing substantially. This development is mainly caused by burning of fossil fuels. The origins of the anthropogenic $CO_2$ emissions are listed in table 3.1 below.

| | Source |
|---|---|
| 25.9% | Energy supply |
| 19.4% | Industry |
| 17.4% | Forestry |
| 13.5% | Agriculture |
| 13.1% | Transport |
| 7.9% | Residential, comercial buildings |
| 2.8% | Waste and wastewater |

**tab.3.1** Source distribution for anthropogenic $CO_2$emissions. Source: IPCC-AR4.

Methane has increased as a result of human activities related to agriculture, natural gas distribution and landfills. Natural emissions occur, for example, in wetlands. In 2005, methane had a global average concentration of 1774 ppb.

Nitrous oxide is also emitted by human activities such as fertilizer use and fossil fuel burning. Natural processes in soils and the oceans also release $N_2O$. In 2005, nitrous oxide had a global average mixing ratio of 319 ppb.

Halocarbon gas concentrations have increased primarily due to human activites. Principal halocarbons include the chlorofluorocarbons (e.g., CFC-11 and CFC-12), which were used extensively as refridgeration agents and in other industrial processes before their presence in the atmosphere was found to cause stratospheric ozone depletion. The abundance of chlorofluorocarbon gases is currently decreasing as a result of international regulations designed to protect the ozone layer.

Ozone is a GHG that is continually produced and destroyed in the atmosphere by chemical reactions. In the troposphere, human activities have increased ozone through the release of gases such as carbon monoxide, hadrocarbons and nitrogen oxide, which chemically react to produce ozone.

Water vapour, although being the most abundant and important GHG in the atmosphere, is only to a small extent directly influenced by human activities. However, water vapor is indirectly influenced by a changing climate, since changes in atmospheric temperature result in a different capability of the atmosphere to contain water vapor. Surface specific humidity as well as total column water vapor have increased globally consistent with the recent warming of the atmosphere. Additional water vapor contributions come from emissions of methane, which undergoes chemical destruction in the stratosphere, producing a small amount of water vapor. Thus water vapor may cause larger climate changes than due to $CO_2$ alone and changes in atmospheric humidity should be accounted for in modeling climate change.

Aerosols are small atmospheric particles with widely varying size, concentration and chemical composition. Some aerosols are emitted directly into the atmosphere while others are formed from emitted compounds. Fossil fuel and biomass burning have increased aerosols containing sulphur compounds, organic compounds and black carbon (soot). Human activities such as surface mining and industrial processes have increased the amount of dust in the atmosphere.

Referring to the calculated radiative forcings of the various natural and anthropogenic forcing agents, which were summarized in the IPCC-AR4, changes in carbon dioxide cause

a radiative forcing almost equal to the sum of all forcings, meaning that the remaining forcing agents almost cancel each other with respect to their - partially negative - radiative forcings. The reasons that the $CO_2$ variations have so often been assumed to be causes of climatic variations may be: 1) The $CO_2$ content of the atmosphere is so remarkably uniform over space and time that it is possible to observe long-range variations in its mean value. This is impossible for almost any other factor which can influence the radiation processes. Cloudiness, water vapour, and temperature show strong variations with day, season, latitude, and between oceans and continents. 2) The influence of $CO_2$ variations on the long-wave radiation seems to be evident because its physical mechanism is relatively clearly understood. Thus this work will concentrate on $CO_2$ as the cause of climate change, rather than accounting for all the remaining forcing agents.

Ramaswamy et al. (2001) define radiative forcing as 'the change in net (down minus up) irradiance (solar plus longwave; in $W/m^2$) at the tropopause after allowing for stratospheric temperatures to readjust to radiative equilibrium, but with surface and tropospheric temperatures and state held fixed at the unperturbed values'. Radiative forcing can be related through a linear relationship to the global mean equilibrium temperature change at the surface $\Delta T_S$: $\Delta T_S = \lambda * RF$, where $\lambda$ is the climate sensitivity parameter.

It is generally agreed that increasing atmospheric $CO_2$ will lead to higher atmospheric temperature, and global temperature changes corresponding to a doubling of $CO$ have been estimated at about 2-3K. The predicted temperature changes are largest at high latitudes and it has been suggested that one of the first effects may be the melting of the polar ice sheets. However, the resulting temperature changes are not only an effect of an increased net longwave radation. If the additional radiation at the surface from increased $CO_2$ is balanced by additional longwave radiation emitted from the surface, the surface temperature must rise following the "black radiation" curve. If the additional energy is balanced by latent heat liberation, the associated temperature rise is evidently much smaller. Feedback mechanisms can amplify or dampen the response to a given forcing. There are many feedback mechanisms in the climate system that can either amplify ('positive feedback') or diminish ('negative feedback') the response to a change in climate forcing.

The most obvious feature of global warming is the pattern of land-sea contrast (see chapter 1). As pointed out by Manabe et al. (1991), over sea or wet surfaces it is likely that much of the additional energy will be used to enhance evaporation (since evaporation is very sensitive to changes in surface temperature, as a consequence of the Clausius-Clapeyron relationship). The energy budget will therefore be substantially balanced by an enhanced upward latent heat flux. By contrast, over a comparatively dry land surface there is much less potential to enhance evaporation, thus a greater portion of the additional energy will be used to raise the temperature. The energy budget will then be balanced by the resultant enhanced upward sensible and longwave heat fluxes (which are less sensitive than is the latent heat flux to changes in surface temperature). This simple argumentation neglects many possible complexities. For instance, feedbacks related to lapse rate, water vapour, cloud and albedo might well differ over land and sea. The surface forcing may also differ, e.g. as a consequence of the humidity contrast between land and sea. However, the point of the argumentation is to suggest how the different nature of the land and sea surface might explain the greater warming over land than sea.

# Chapter 4

# A simple model for the global surface warming pattern

In this chapter the details of the developed simple climate model will be presented. One of the main purposes of the model is to show that even with a reduction in model equations and simplification of physical processes it is possible to gain a result

In order to keep te model simple several empirical and relatively crude relationships are involved, which were partially drawn from observational or model data sets.

## 4.1 Model domain

The approach to mathematical modelling of the climate is to relate each variable to the others in such a way that changes in one variable involve simultaneous variations in others that in turn have a feedback effect on the original variable.

The model domain is a simple two-layer system consisting of the earth's surface and an artificial atmospheric layer. Both layer have a horizontal resolution of 2.5° in longitude as well as latitude. Within the surface layer ocean and land are treated separately (using a land-sea mask), because the heat capacity of the land surface layer ($C_L$)is much less than over the ocean mixed layer ($C_W$) (see next section).

## 4.2 General equations

### 4.2.1 Temperature equations

We formulate the problem as an initial value problem in which the basic energy balance equations are integrated from a given initial state until a final asymptotic equilibrium state (i.e. climate) is obtained. In order to set up a simple energy-balance climate model the surface temperature is used as the principal dependent variable and it is assumed that all energetic fluxes can be parameterized by the temperature at the earth´s surface, which is a crucial simplifying assumption. The energy balance equation may be written in a time-dependent form:

$$C\frac{dT}{dt} = (1-\alpha) * \bar{S}(\varphi, t) - (1-g)\epsilon\sigma T^4 + Q_{lat} + Q_{sens} + F \tag{4.1}$$

$$C_{atm}\frac{dT_a}{dt} = Q_{lat_{atm}} - Q_{sens} + D * \nabla^2 T_a + \vec{v} \bullet \bigtriangledown T_a \tag{4.2}$$

where C is the thermal inerta coefficient (heat capacity) for a column of the relevant layer within the earth-atmosphere system. The terms in the energy equation have units of energy per unit area per unit time $(W/m^2)$. The energy flux equations contain the storage of energy and the horizontal transport (diffusion) of heat in the oceans and in the troposphere, the excess of radiation at the surface of the earth, the sensible heat given off from the surface to the troposphere, the heat lost by the ground due to evaporation and the heat gained by the troposphere by condensation of water vapour in the clouds. These equations coupled with the ice-albedo condition and simple boundary conditions at the poles, completely specify the problem, that is solved for the surface temperature field. The solution was extracted by reliable numerical procedures. The time step for integration is choosen to be $\Delta t = 1day = 86400s$. One is then in a position to vary such 'given' parameters as the solar constant to study the model response.

The value of C could also be interpreted as a scaling factor for the time scale t that a system needs to recover from a perturbation back to equilibrium. A rule of thumb is that any positive feedback will increase the timescale for equilibration. However, the value of c does not change the final steady state of the model. For the ocean the heat capacity was calculated assuming a mixed layer of 50m depth, whereas the land surface layer is assumed to have a thickness of 2m. Thus an effective heat capacity is given by:

$$C_{ocean} = c_{p_{ocean}} * m = c_{p_{ocean}} * \rho_{ocean} * V \tag{4.3}$$

$$C_{land} = c_{p_{land}} * m = c_{p_{land}} * \rho_{land} * V \tag{4.4}$$

where $c_{p_{ocean}} = 4186 \frac{J}{kg*K}$ (value for water at T=15°C), $\rho_{ocean} = 999.1 \frac{kg}{m^3}$ (at 15°C) and V=50m$^3$. The spacific heat of dry land is approximately 4.5 times less than that of the ocean (for moist land approx. 2 times less) and the layer thickness was taken as 2m with an density of $\rho_{land} = 2600 \frac{kg}{m^3}$ (value for solid rock). Thus a ratio of both layers heat capacities of approximately 43 was attained: $\frac{C_{ocean}}{C_{land}} \cong 43$. Wihtin a seasonal cycle the greater heat capacity of the ocean would cause a delayed maximum in surface temperatures respetive to land temperatures. If the climate is changing over a longer time period the ocean will need significantly more time to equilibrate to the changed forcing than the land surface.

For the atmosphere as a whole the heat capacity is $C_{atm} \approx 5 * 10^{21} \frac{J}{K}$. Deviding by the earth's surface area of A=5.1*10$^{14}$ m$^2$ yields the heat capacity for an atmospheric column of 1m$^2$ ground area of $C_{atm} = 10^7 \frac{J}{Km^2}$.

### 4.2.2 Humidity equation

The atmospheric amount of water vapor is influenced by evaporation from the surface moisture reservoir and by precipitation, as well as by the atmospheric transport which consists of lateral diffusion and horizontal advection by the mean wind field:

$$\frac{dq}{dt} = \Delta q_{lat} + \Delta q_{prec} + + D * \nabla^2 q + \vec{v} \bullet \bigtriangledown q + \Delta q_{corr} \tag{4.5}$$

Since this is a simple climate model based an parameterizations, there is an additionally correction term, which enables the model to reproduce present climate conditions (see section 4.7). For the calculation of the water vapor flux associated with evaporation see section 4.5.2 . An exponential decay is assumed for the removal of water vapor due to precipitation. Water vapor has an average residence time within the atmosphere of approximately 10 days. This yields a relation as

$$\Delta q_{prec} = -0.9048 * q \tag{4.6}$$

for a time step of one day.

A flux correction term according to the humidity climatology is completing the equation.

## 4.3 Solar radiation

### 4.3.1 Seasonal cycle of solar insolation

The seasonal and geographical pattern of solar insolation was calculated by following the equations in section 2.1. Thus the daily cycle of solar radiation reaching the top of the atmosphere was calculated for each day of the year and for each grid point. Then the amount of radiation is integrated over the length of day (from sunrise to sunset ($\theta = 90$)). This is done by setting equation (2.4) equal to one, yielding:

$$t = \arccos\left(\frac{1 - \sin\varphi * \sin\delta}{\cos\varphi * \cos\delta}\right) = t\,(\varphi, JD) \tag{4.7}$$

The claculations produced the pattern of solar energy input shown in figure 4.1.

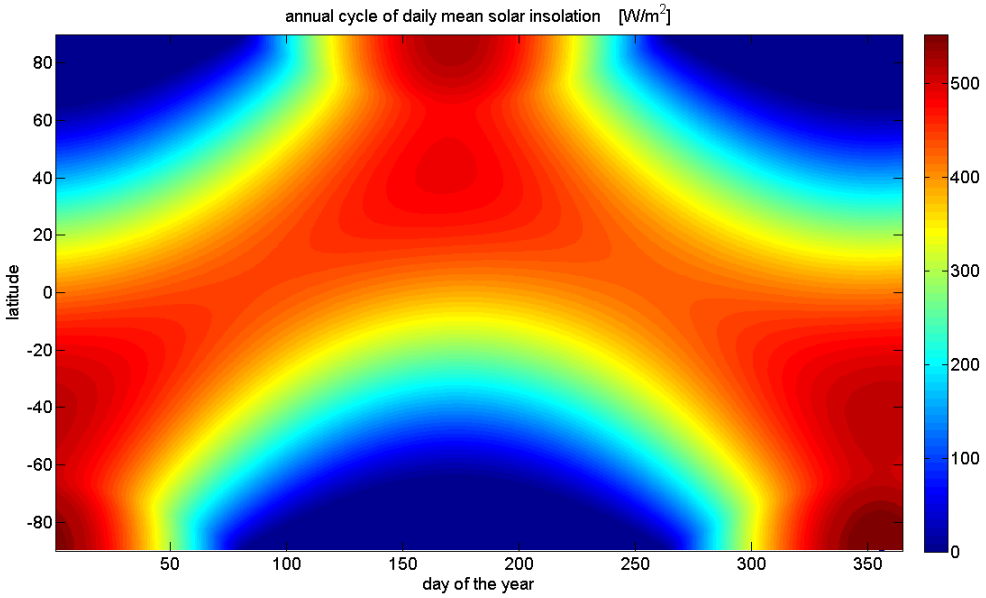


**fig.4.1** The seasonal and latitudinal distribution of daily mean amount of solar radiation.

A difficulty in calculation arises poleward of 66° latitude, where cos$\theta$ approaches either zero when the sun is continuously above the horizon in summer or it approaches one during polar night. Poleward of this border the daily sum of direct solar radiation equals zero (polar night), whereas in the respetive summer polar region the solar radiation reaches a seasonal as well as a regional maximum, which is, however, strongly influenced by the elevation angle.

Indeed, if one takes the average over all latitudes and over the year of the described pattern one gets a value equalling one-quarter of the solar constant (342 W7m$^2$). Thus this calculation is consistent with other global and annual mean consiadarations. The calculated S($\varphi, JD$) pattern was then given as an imput data set for the model.

### 4.3.2 Albedo formulation

Since the surface coverage with snow or ice is to a first order controlled by the temperature, the corresponding surface albedo can be handeled as a function of temperature. We adopt an albedo description similar to that used by both Sellers and Budyko, which seems intuitively reasonable. One assumes that the boundary of the polar ice cover (and local ice or snow regions) corresponds to a definite temperature near the earth´s surface. If T(x) is less than -10°C ice will be present, while if T(x) is greater than 0°C there will be no ice. In the intermediate temperature interval a linear increase in albedo with decreasing temperature is assumed. This is a parameterized mimic of the observed fact that a decrease in the surface temperature in mid or high latitudes would usually be accompanied by an increase of snowfall or sea ice formation, and therefore an increase of surface albedo. The converse would apply for an increase of surface temperature. When this condition is coupled with the energy balance equation, the system becomes highly nonlinear. This nonlinearity is known as the ice-albedo feedback mechanism.

The albedo of the surface of the earth is assumed to have the values described in the simple climate model of Budyko (1968). A value of 0.3 is taken for ice-free regions and 0.6 for ice-covered regions both 50% covered with clouds. Thus the change of surface conditions from ice-covered and ice-free can cause a change in albedo of about 0.3.

$$\alpha_{ice}\left(T \leq 263K\right) = 0.6 \tag{4.8}$$

$$\alpha\left(263K < T < 273K\right) = a_{ice} - \frac{\alpha_{ice} - \alpha_{icefree}}{10K}(T - 263.15K) \tag{4.9}$$

$$\alpha_{icefree}\left(T \geq 273K\right) = 0.3 \tag{4.10}$$

Thus the albedo of the tropical regions is not affected by a temperature change in the albedo formulation unless the temperature of the tropical regions, which initially (and presently) is about 300K, becomes considerably colder (at least 27K colder) than they are at present. However, a slight decrease in temperature in temperate and higher latitudes (where T$<$273K) would cause a significant positive feedback, whereby the albedo of these temperate or polar regions would become considerably higher. Once a complete ice or snow cover is reached at temperatures below 263K the albedo is not further enlarged.

The albedo-temperature formulation used in this models does not explicitly include coupling to the hydrological cycle, including cloud processes. The effects of variations in cloud cover on the albedo were ignored, mainly because there is no easy way to include them. It is possible that satellite observations (which include cloudiness effects as well as surface albedo) would suggest a functional relationship between albedo and surface temperature different from the linear one.

The albedo of continental ice sheets were treated seperately from the above relationship. Since the massive continental ice caps of Antarctica and Greenland are generally believed to vary on time scales of millennia they may be specified as given external boundary conditions for calculations on shorter time scales. Thus the albedo of Greenland and Antarctica are held constant at the value for ice-covered regions (0.6).

## 4.4 Greenhouse effect parameterization

Since the model will be applied for global warming scenarios and a central aspect will be the anthropogenically induced greenhouse feedback due to increased $CO_2$ concentrations, the formulation of the longwave radtion scheme is a central element of the model. Due to

the restricted domain of the model, where only two layers are available to represent the processes making up the greenhouse effect, it is necessary to fall back upon a parameterization. Parameterization (short for parametric representation) is a technique of relating the statistical effects of processes (being related to average conditions over much longer periods and scales) that cannot be computed in detail to those processes that are computed in detail.

An empirical formula was obtained using model output data from an ECHAM5 $CO_2$ experiment, which was carried out only for this purpose. The strength of the greenhouse effect locally depends on various parameters such as the surface temperature, the atmospheric humdity and the atmospheric $CO_2$ concentration. The letter can to first order be assumed to be globally constant.

Thus an equation was determined that relates the net longwave radiation at the surface to the surface temperature (T), the atmospheric humidity and the global mean concentration of $CO_2$. The atmospheric humidity is represented by the vertically integrated amount of water vapor (given in units of $kg/m^2$). Whereas the surface temperature, the net longwave radiation and the vertically integrated water vapor are output data sets of the applied model, the $CO_2$ concentration was used as an input parameter for the experiments taken out. According to Ramaswamy et al. (2001) for $CO_2$ radiative forcing increases logarithmically with mixing ratio. Thus the values for the $CO_2$ concentration used in the experiments were chosen according to a logarithmic increase from 200ppm and 1000ppm (see table 4.1). At present the atmospheric $CO_2$ concentration is around 380ppm. Thus a doubling of $CO_2$ is still within the choosen interval of the experiments and the calculated parameterization is valid for the aspected $CO_2$ values occuring in the model.

| $c_{CO_2}$ [ppm] | 200 | 239 | 286 | 342 | 409 | 489 | 584 | 699 | 836 | 1000 |
|---|---|---|---|---|---|---|---|---|---|---|

**tab.4.1** Carbon dioxide cancentrations choosen for a ECHAM5 experiment to generate data for a parameterization calculation of the greenhouse effect. A logarithmic increase is choosen since the relation is known for the radiative forcing depending on $CO_2$

From the model output only the data for january and july were used to cover the seasonal cycle using a data set as small as possible. From the gathered data a relation was determined for a 'greenhouse parameter', g, that will be characterizing the strength of the greenhouse effect in the developed model. It represents the effect of water vapor and $CO_2$ on the longwave radiation balance of the earth-atmosphere system:

It is assumed that the portion of the surface longwave radiation that is reemitted by the atmosphere is proportional to the surface temperature. This assumption surely is crucial, but it simplifies the problem a lot:

$$nLW = LW \uparrow + LW \downarrow = -\sigma T^4 + g * \sigma T^4 = -(1-g)\sigma T^4 \tag{4.11}$$

Here nLW denotes the surface net longwave radiation being the sum of the emitted and received longwave radiation. The global average value of nLW is in general negative with an absolute value in the order of 50-60$\frac{W}{m^2}$. Within the seasonal cycle this value is higher in July than in January. Corresponding to the results of these experiments the nLW absolute value decreases as the global $CO_2$ concentration increases, meaning that the surface looses less thermal energy. This fits to the general projections for a global warming scenario, whereas the surface temperature raises in accordance. Solving equation (4.9) for g yields:

$$g = 1 + \frac{nLW}{\sigma T^4} \tag{4.12}$$

Now, with a decrease in the absolute value of nLW and a simultaneous increase in surface temperature (T) the value of g is increasing according to eq. (4.10). Thus a higher value of g corresponds to a stronger greenhouse effect.

Subsequently to these calculations of the greenhouse factor g a parametrization was calculated by fitting the data to the corresponding values of the vertically integrated water vapor (VIWV) and the atmospheric $CO_2$ concentration:

$$g\left(VIWV, CO_2\right) = a_1 + a_2 * \log\left(VIWV\right) + a_3 * ln\left(\frac{CO_2}{c_0}\right) \tag{4.13}$$

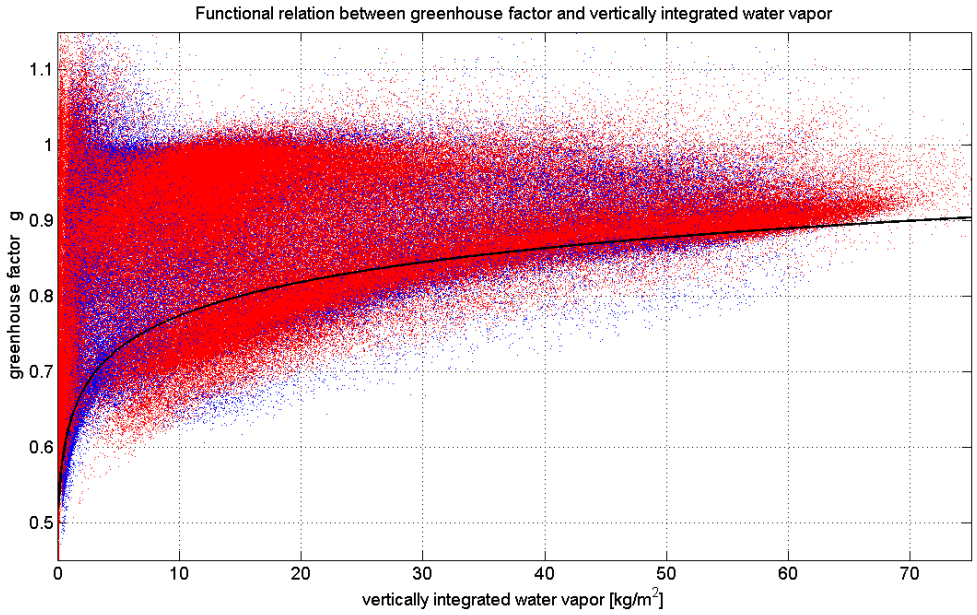


**fig.4.2** Scatter plot between vertically integrated water vapor and the calculated greenhouse factor used in the model. The data are drawn from an ECHAM5 $CO_2$ experiment. Red and blue markers represent data values for July and January, respectively. The calculated regression function is shown as a black line follwing the lower branch of the data cloud. Data values above this branch are assumed to be caused by "warm air advection" and are ingored when calculating the regression function.

A fixed parameter is the mean $CO_2$ concentration within the time period 1950-1999, which has the value $c_0 = 340ppm$. The coefficients $a_i$were determined by regressing the data to this equation (see figure 4.2). The result is: $a_1 = 0.617 \pm 0.001$, $a_2 = 0.065 \pm 0.001$ and $a_3 = 0.006 \pm 0.0002$ (uncertainties correspond to the 95% confidence interval). Physically, this means that the greenhouse effects strengthens as VIWV and $c_{CO_2}$ increase, since the corresponding parameters $a_2$and $a_3$ are positive. This agrees with global warming projections.

However, when the developed simple model was run with the just calculated parameterization for the greenhouse factor it was not able to reach a stable equilibrium state. A somewhat too strong sensitivity of g for water vapor changes is causing to high humidity increases which in turn causes stronger temperature increases and thus induces an instable water vapor feedback. To prevent the model from getting unstable, a compromise was made by reducing the coefficient that determines the sensitivity of the greenhouse factor to water

vapor. This, of course, is a very crucial but necessary procedure und the present simple state of the model. This led to the following relation, which was than used for all further calculations:

$$g\left(VIWV, CO_2\right) = 0.617 + 0.04 * \log\left(VIWV\right) + 0.006 * ln\left(\frac{CO_2}{c_0}\right) \tag{4.14}$$

## 4.5 Latent and sensible heat flux parameterizations

### 4.5.1 Latent heat flux

For the latent heat flux a Bulk formula was used for parameterization of the process:

$$Q_{lat} = \rho_{air} * L * u * C_q * (q_{air} - q_{sat}) \tag{4.15}$$

with the air density of air $\rho_{air}$ $[\frac{kg}{m^3}]$, the latent heat of evaporation L $[\frac{J}{kg}]$, the wind speed u $[\frac{m}{s}]$, the Bulk transfer coefficient for latent heat $C_q$ [dimensionless], the specific humidity of the surface air layer $q_{air}$ $[\frac{kg}{kg}]$ and the saturation specific humidity $q_{sat}$ $[\frac{kg}{kg}]$. The letter is calculated from the surface temperature based on the Clausius-Clapeyron relation: The saturation water vapor pressure E only depends on the temperature:

$$E\left[hPa\right] = 6.1078hPa * \exp\left(\frac{17.08085 * (T - 273.15K)}{234.175K + T}\right) \tag{4.16}$$

The saturation specific humidity ($q_s$) is to a first order proportional to the saturation vapor pressure (E) (taken from DWD, 1987):

$$q_s = \frac{622 * E}{p - 0.378 * E} \approx 622\frac{E}{p} \tag{4.17}$$

Here p denotes the atmospheric pressure in units of hPa, which has a global average surface value of 1013.25hPa.

According to Rapti (2005) the specific humdity of the air near the surface can assumed to be proportional to the vertically integrated amount of precipitable water. This also holds in the data set from the model experiment mentioned in section (4.4), since, as shown in figure 4.3, the vertically integrated water vapor obviously exponentially depends on the surface temperature. Thus, for the simple climate model, the specific humidity q (being a variable in the model) and the vertically integrated water vapor (used in the greenhouse effect parameterization) are also assumed to be proportional, with a determined relation:

$$VIWV = 2.6736 * 10^3 * q \tag{4.18}$$

The latent heat of evaporation has a value of $2257\frac{kJ}{kg}$ at a temperature of 100°C and an atmospheric pressure of p=1013.25hPa. This value is used in the model independently of the temperature. The wind speed is taken as a constant mean value of u=$6\frac{m}{s}$. Thus the pattern of the global wind field will not affect the model result. The transfer coefficient $C_q$ was scaled in a way that $C_{q_{ocean}} = 10 * C_{q_{land}}$ in order to account for the reduced potential evaporation over land.

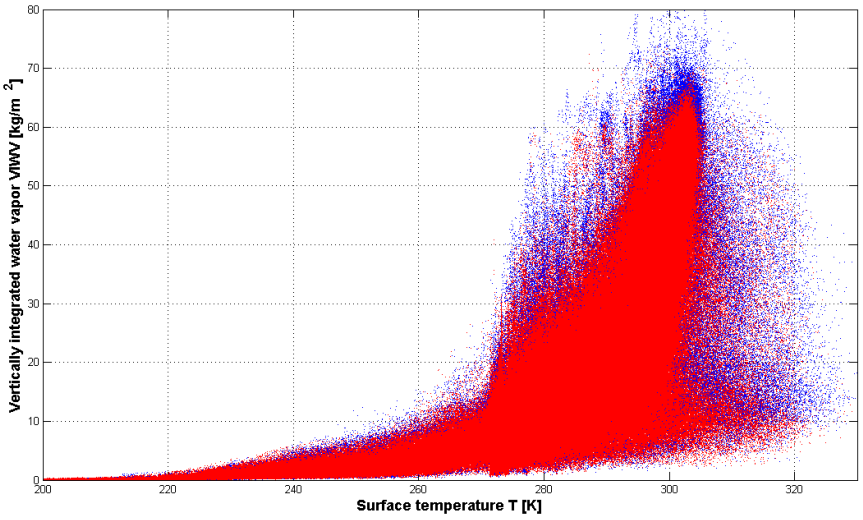


**fig.4.3** Relation between surface temperature and vertically integrated water vapor from data gained by an ECHAM5 $CO_2$-experiment. As known for saturation water vapor or saturation specific humidity, the vertically integrated water vapor can also be seen as being proportional to some exponential function of surface temperture. This has been assumed in the simple model.

Once the latent heat is lost by the surface and transported into the atmosphere in the form of water vapor it eventually is released in accordance to precipitation. As already mentioned in section 4.2.2 the atmospheric humidity is assumed to have an average residence time of ten days and thus follows an exponential decay which is interpreted as precipitation. The daily amount of precipitation is than used to calculate the latent heat release within the atmospheric layer:

$$Q_{lat_{atm}} = -\Delta q_{precip} \bullet L \tag{4.19}$$

where L denotes the latent heat of water vapor condensation. This amount of heat is used to heat up the atmosphere, which is then coupled to the surface via the sensible heat flux.

### Soilmoisture

Since on land surface the reservoir of water that may be evaporated is not homogeneously distributed, one has to consider the soilmoisture for the calculation of latent heat flux. Especially in desert regions (e.g., Sahara) or polar latitudes the potential evaporation is quite low. Therefore, an additional factor was included in the parameterization for latent heat flux:

$$Q_{lat} = \rho_{air} * L * u * C_q * (q_{air} - q_{sat}) * f \tag{4.20}$$

Here the factor f, which may vary between zero and one, is the measure for the soilmoisture. This value was taken from the soilmoisture field of the ECHAM5-CO2 experiment (see 4.4) under an atmospheric $CO_2$ concentration of 342ppm. As can be seen in figure 4.4 the soilmoisture on land varies between zero and nearly 1m. This makes it suitable for using the soilmoisture as scaling factor for latent heat flux. Thus over land the latent heat flux in the model is not only dependent on surface temperature (via $q_s$) and atmospheric humidity (q), but also on the soilmoisture. Over the ocean soilmoisture was set f=1.

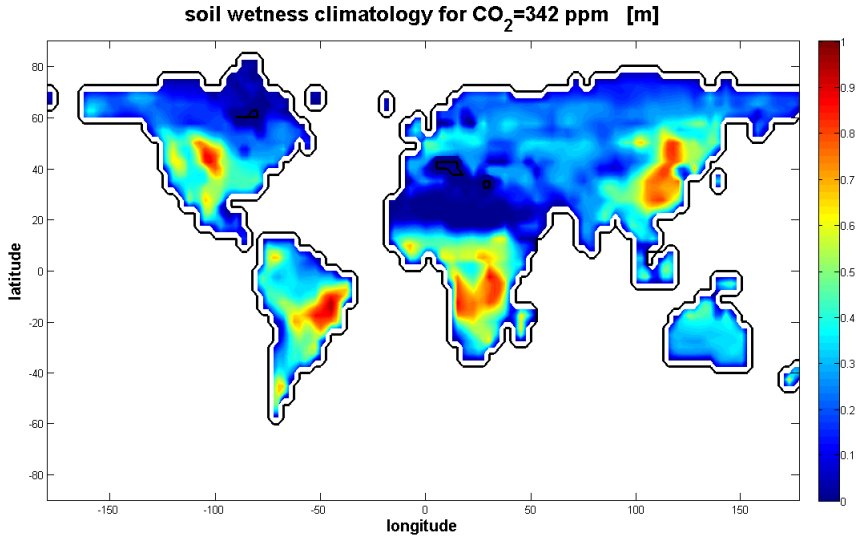


**fig.4.4** Soilmoisture climatology that is used in the simple model. Data are taken from an ECHAM5 simulation and are averaged over a year.

### 4.5.2 Water vapor flux

Latent heat flux at the surface is necessarily connected with an corresponding water vapor flux. Hence, as water vapor evaporates the surface is cooled and the atmospheric layer adjacent to the surface gains a certain amount of water vapor. This water vapor flux is proportional to the latent heat flux:

$$\Delta\left(VIWV\right) = \frac{Q_{lat} * \Delta t}{L} \tag{4.21}$$

Here $\Delta t$ is the time step of integration and $\Delta\left(VIWV\right)$the corresponding change in water vapor resulting from surface evaporation within this time period.

### 4.5.3 Sensible heat flux

Since the atmospheric layer in the model domain rather has an artificial character, it is not appropriate to use an usual parameterization for the sensible heat flux as is applied for the latent heat flux. Of course there is an analogous Bulk formula (see equation 2.13). Instead, a simple approximation was used:

$$Q_{sens} = c_s * (T_a - T) \tag{4.22}$$

The coupling coefficient $c_s$was chosen in a way that the global and annual mean value of sensible heat flux in the control run almost equal the climatic value.

The sensible heat flux implemented in the model is supposed to have no impact on the absolute change of temperature under climate change conditions. It only serves as a coupling between surface and atmosphere. Since $c_s$ does not vary geographically all points are equally coupled between surface and atmospheric layer.

## 4.6 Atmospheric transport: horizontal advection and lateral diffusion

It is necessary to parameterize the horizontal redistribution of energy by atmospheric and oceanic transport. Consider the horizontal transport of (sensible) heat and atmospheric water vapor (latent heat) by the geophysical fluid system, i.e. the atmosphere and the ocean. In the treatment of this transport one has to make drastic idealizations to keep the mathematics simple and manageable. According to Gal-Chen (1975) the "simplest" parameterization is the one which does not distinguish between various (i.e. ocean, atmosphere or latent heat) transport terms.

In this simple model, the atmospheric transport of temperature and humidity is build up of two components: horizontal advection by a mean wind field and lateral diffusion.

### 4.6.1 Lateral diffusion scheme

For a first approximation of the atmospheric redistribution of temperature and humidity the transport term adopted in this model is based upon a turbulent diffusion approach and has the form:

$$\frac{dT}{dt} = D * \nabla^2 T = D * \left( \frac{d^2T}{dx^2} + \frac{d^2T}{dy^2} \right) \tag{4.23}$$

where D is an empirical diffusion coefficient, which is taken to be only latitude-dependent. The diffusion process is assumed to be isotropic meaning that the diffusion follows equally in all directions. Thus, the heat transport is proportional to the negative gradient of temperature or in other words: the net heat transported into a box is proportional to the divergence of the heat flux. Therefore the energy balance equation is a differential equation requiring boundary conditions at the poles (see section 4.6.1.2).

In order to find a realistic constant for the diffusion of energy as a representation for advection the diffusion coefficient is adjusted to the observed present climate by phenomenologically describing the heat transport. It is assumed that thus the model is incorporating the correct basic physics of large-scale atmospheric transport. The diffusion coefficient, which is a measure for the strength of diffusion, was adjusted in a way that regional features of a length scale of approximately 1000km decays in a time period of the order of 10 days. These are typical scaling factors of mid-latitude baroclinic eddies, that contribute to a large-scale mixing of differently heated air masses.

However, it seems unlikely that such a complex phenomenon as latent heat transport, which involves among other things moist convection in the tropics, can be parameterized simply in terms of the local relative humidity, Clausis-Clapeyron relation, and the local temperature gradient. Yet, we concede that it is the differential heating which fundamentally drives the atmospheric motions and therefore one may speculate that the total heat transport may be parameterized as some function of the temperature gradient alone.

#### 4.6.1.1 Method of solution

There exist several different numerical methods to solve the differential diffusion equation. However they strongly depend on the initial and boundary conditions.

The equation is solved numerically by an iterative method.

Applying centered differences in time and space to the Laplacian operator leads to the following formulation of the diffusion model:

$$\frac{d^2T}{dy^2}(j,k) \approx \frac{T_{j,k-1} - 2T_{j,k} + T_{j,k+1}}{\Delta y^2} \tag{4.24}$$

In order to increases the models stability a higher order discretization scheme, where the central differences were averaged over seven successive grid points, was applied in longitudinal direction.:

$$\frac{d^2T}{dx^2}(j,k) \approx \frac{1}{20}\frac{1}{\Delta x^2}\,(\,[T_{j-3,k} - 2T_{j-2,k} + T_{j-1,k}] + 4\,[T_{j-2,k} - 2T_{j-1,k} + T_{j,k}]$$

$$... + 10\,[T_{j-1,k} - 2T_{j,k} + T_{j+1,k}]$$

$$... + 4\,[T_{j,k} - 2T_{j+1,k} + T_{j+2,k}]$$

$$... + [T_{j+1,k} - 2T_{j+2,k} + T_{j+3,k}]\,) \tag{4.25}$$

The spatial as well as temporal resolution used in the diffusion scheme has to be adjusted in a way that the model is prevented from getting unstable. Thus within the diffusion scheme a shorter time step $\Delta t_{diffusion} = \frac{1}{4}day$ is used than in the general integration. However, in higher latitudes the diffusion model tends to get unstable under these conditions of temporal and spatial (2.5°) resolution. For this reason a variable time step was introduced, that is decreasing with increasing latitude:

$$\Delta t_{diffusion} = \Delta t_0 * min\left(1, \frac{D * \Delta t_0}{dx_\varphi^2}\right) \tag{4.26}$$

with $\Delta t_0 = \frac{1}{4}day$ and $dx_\varphi^2$ is the latitude dependent longitudinal resolution. For the adjusted diffusion coefficient a value of $5{*}10^5 \frac{m^2}{s}$ was choosen. Thus poleward of about 60° laitude the time step for the diffusion subroutine is continuously decreasing.

#### 4.6.1.2 Boundary conditions

In order to solve the energy balance equation we must constrain the solution by boundary conditions: no heat transport is allowed across the poles. Since heat flux is proportional to the gradient of T(x,y), the horizontal gradients of temperature must vanish at the poles:

$$-D\frac{dT}{dy} = 0 \tag{4.27}$$

This is done by introducing two points at $\varphi$=-92.5° and $\varphi$ =92.5° at which the sea level temperature is set equal to $T(\varphi = -90)$ and $T(\varphi = 90)$, respectively. By doing so, the following discretizations are applied at the polar boundaries of the model grid:

for the southern boundary (k=1)

$$\frac{d^2T}{dy^2}(j,k) \approx \frac{-T_{j,k} + T_{j,k+1}}{\Delta y^2} \tag{4.28}$$

and for the northern boundary (k=ydim)

$$\frac{d^2T}{dy^2}(j,k) \approx \frac{T_{j,k-1} - T_{j,k}}{\Delta y^2} \tag{4.29}$$

Thus one systematically eliminates an unphysical solution that diverges at the poles.

### 4.6.2 Horizontal advection

Since the diffusion approach is not able to give a sufficiently realistic picture of the horizontal atmospheric transport with respect to wind dierection and amplitude the transport term was extended by an advection scheme, which has been developed by Dietmar Dommenget. A NCEP climatology for the wind field in the 850 hPa level is adopted for the atmospheric advection. In figure 4.5 the corresponding wind pattern is shown.

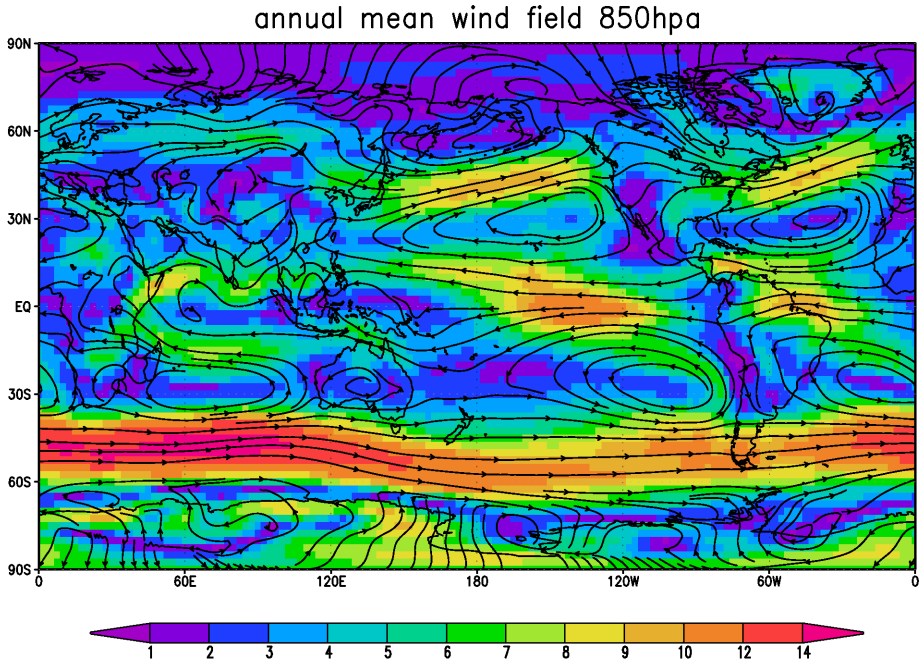


**fig.4.5** Annual mean horzontal wind in 850 hPa. Streamlines and absolute values (unit $\frac{m}{s}$) are shown. Data are taken from a NCEP climatology.

According to this additional atmospheric transport mechanism the diffusion coefficient has been reduced to $2*10^5 \frac{m^2}{s}$

## 4.7 Input data, parameters and flux correction

### 4.7.1 Input data: climatologies

In order to achieve a simple climate model that is able to reproduce the current climate as a steady state solution, a NCEP data set of surface temperature was applied as a reference (see figure 4.6). This climatology was calculated from the monthly mean temperature series from 1948 to 2004 and interpolated on a daily basis. Thus for each time step integrated in the model there is a refrence temperature available for comparison. Analogously, a climatology for atmospheric specific humidity was used, which was calculated from the NCEP reanalysis of montly mean precipitable water content (see figure 4.7).

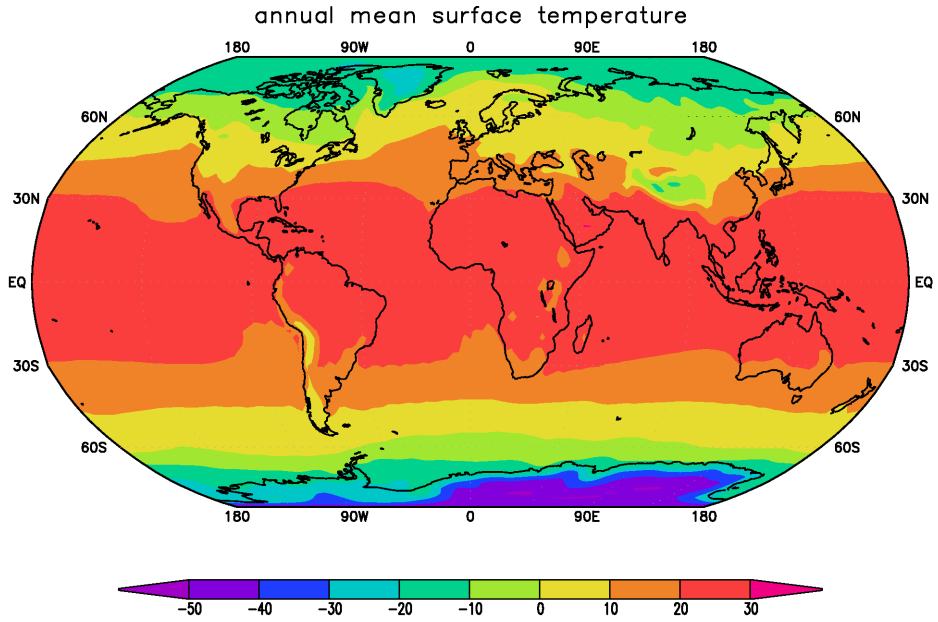


**fig.4.6** Reference annual mean surface temperature climatology (degree Celsius). Data taken from NCEP.

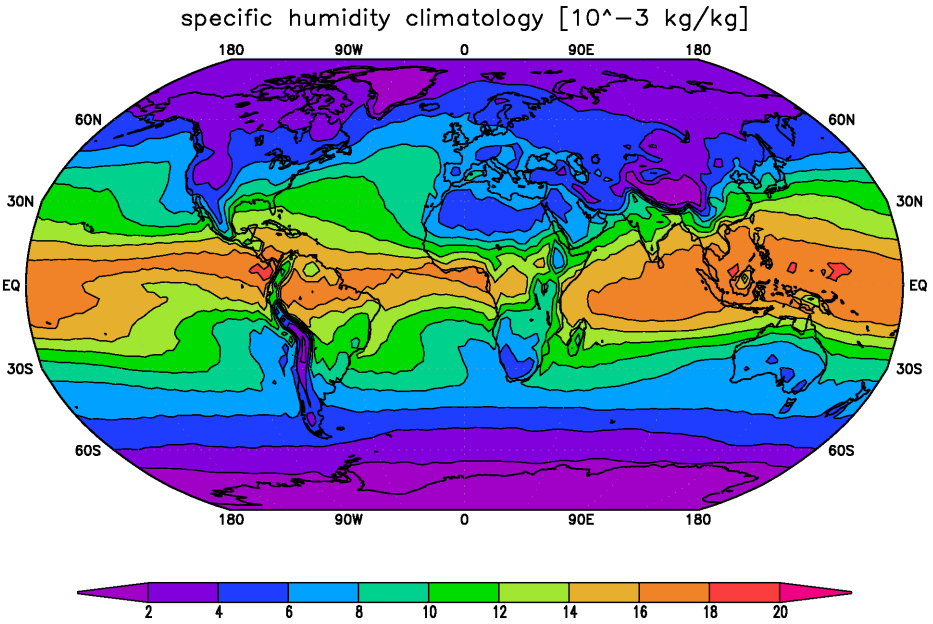


**fig.4.7** Reference climatology for specific humidity

As is known fro climatological observations surface temperature as well as atmospheric humidity show a maximum in the tropics and decrease towards the poles. This is due to

the latitudinal variation of solar insolation as well as to the water vapor feedback which certainly is the central coupling between the two climate parameters.

For the humidity climatology an additional condition was introduced in order to prevent the model from getting oversaturated with respect to humidity, which is physically quite unprobable:

$$q_{clim} = min\left(q_{NCEP}, 0.95 * q_s(T_{NCEP})\right) \tag{4.30}$$

Here the climatological saturation specific humidity is calculated from the corresponding NCEP data for surface temperature. Thus the humidity climatology is consistent with that of the surface temperature.

### 4.7.2 Parameters

The following values are adopted as standard values for the terrestrial atmosphere:

- air density: $\rho_{air}$ =1.2 kg/m$^3$
- atmospheric concentration of carbon dioxide: 340ppm (present-day) and 2*340ppm (global warming scenario)

### 4.7.3 Flux correction

Most AOGCMs adopted in the current IPCC report no longer use flux adjustments, which were previously required to maintain a stable climate. Previously it was common to adjust parameter values in order to optimize model simulation of particular variables or to improve global heat balance. This process is referred to as 'tuning'. It is sometimes used to control parameters not to exceed observationally based constraints.

Especially in energy balance models where physics are kept simple tuning the model to the present climate conditions is an often applied procedure. In general this is done by varying the constant(s) in the formulation of the energy transport, for example, on tries to obtain a best fit of the thermal diffusion coefficient to the observed temperature distribution. However, the mere fact that the models reproduce the observed surface temperature distribution cannot be taken as an indication of the validity of the models simply because the models are based on, in fact deliberately tuned to, empirical data.

Nevertheless, the aim of this work is to develop a simple model for the global surface warming pattern. Thus flux correction will be an element, which is hard to be renounced. In order to be able to reproduce the present climate there are correction terms introduced for surface temperature and atmospheric humidity. Thus for both of these variables reference data sets are needed.

## 4.8 Shortcomings of the model

One now has to ask the question "how realistic is the conceptual model?" It must be borne in mind that the results obtained with such simplified empirical parameterizations cannot assuredly be close to reality. Nevertheless, the model does satisfy the energy balance of the earth-atmosphere system, and in the long term it is the energy balance that must determine the surface temperature. This model is at the very least a valuable 'educational toy' giving a "first guess" of what should be expected from much more sophisticated models (atmospheric, oceanic, and joint atmosphere-ocean) that explicitly include detailed hydrological cycle and dynamic calculations.

Although the assumptions made in the model were specified so as to be physically realistic, the possibility still remains that neglected higher order or nonlinear effects could alter the picture considerably. The most obvious shortcoming is the model's failure to incorporate cloudiness as a feedback mechanism. Other feedbacks are also neglected such as nonlinear thermal diffusion, salinity advection in sea water, availability of moisture for producing snow, and so on. A physically much more satisfactory approach is to derive the ice and snow cover from the hydrological cycle. Regionally, the changes in polar ice or snow cover can differ strongly from the area average behaviour, since ice or snow cover are influenced by temperature changes as well as changes in precipitation. These two competing effects can cancel out each other or even result in an increase in local snow or ice cover, since due to increased temperatures and possible increases in precipitation may cause an increase in snow accumulation. This somehow dampens the potenial ice albedo feedback, which otherwise would cause stronger temperature changes. Since the albedo formulation used in this model does not include effect concerning the hydrological cycle it becomes questionable whether one can still use the kind of functional form of temperature albedo. Additionally, surface characteristics changed through human activity can typically change surface albedo by 10%. Such changes could be of more than regional climatological significance.

The dominant factor determining surface temperatures over oceans in his calculation appears to be the upward mixing from the base of the seasonal thermocline, whose temperature is specified. Thus neglecting oceanic processes beyond the mixed layer certainly hinders a simpel model from reproducing all features of climate patterns. Furthermore, climate feedbacks associated with chemical or biochemical processes are not considered.

The skill of the model improve considerably when advection by the mean wind is included. In the real world, moisture convergence will occur at the different levels in the atmosphere, a feature which cannot be reporduced in this model. Thus a more realistic representation of the hydrological cycle would be improving the model further.

Another potential improvment lies in a more detailed representation of the longwave radiation scheme of the model. Since the atmospheric layer is a more artificial structure rather than a representation of a certain level within the atmosphere, it was not possible to come up with a sufficient representation of the longwave radiation emitted from this atmospheric layer. However, this should be attempted in further work, since thus the sensitive parameterization of the greenhouse factor can be improved also.

# Chapter 5

# Model results and discussion

A simple conceptual model was applied and idealized experiments were run in order to explain the global surface warming pattern which is observed in the real climate and shows up in broadly used general circulation models. Since the climate is represented by the long-term averages of atmospheric variables, the discussion will be based on numerically calculated equilibrium states of the model.

Before undertaking this project, it is desirable to answer the following question by performing a series of computations of equilibrium states: How long does it take to reach a climate state of thermal equilibrium? - After running through all model setups (see section 5.2), an equilibrium time of approximately 80 years was determined as being sufficiently long in order to get reliable results.

In order to clarify which physical processes are most important for the surface warming pattern, various different model integrations were carried out and the response patterns were analysed. In the case of forcing experiments the results for each model were differenced from a corresponding control integration (in which radiative forcing is held constant) to remove possible climate drift.

## 5.1 Surface warming pattern

### 5.1.1 Annual mean response pattern to CO2 doubling

The developed simple climate model was now used to calculate the global surface warming pattern that would occur in an equilibrium climate state with a doubled $CO_2$ concentration with respect to the present-day value. Figure 5.1 illustrates the equilibrium response of surface temperature to a doubling in the atmospheric $CO_2$ content from 340ppm to 680ppm. One can see the model result including all implemented processes and most probable values for parameters. The major features of the surface warming patterns suggested by IPCC models are present: A more or less pronounced (depending on latitude) contrast between an amplified warming over land and a dampend warming over the oceans and the polar amplification on the northern hemisphere. Especially on the northern hemisphere (having a considerably higher portion of land masses) within a latitude belt the warming over land is stronger than over the surrounding ocean. The polar amplification of surface warming is clearly visible, however, it seems to be too strong. This probably results from a very strong ice-albedo feedback (see section 5.2.3) and atmospheric transport distributing the strong warming to wider regions.

Another feature is the reduced tropical warming over the continents as well as over the oceans, which results from a local maximum of the latent heat flux acting as a negative

feedback. Due to this feedback one might expect the warming to be higher in regions where land is relatively dry, and lower in regions where land is relatively wet (see section 5.2.2). This pattern agrees with the IPCC results. This local minimum in surface warming also corresponds with the region where high rates of precipitation associated with the ITCZ occur. Over the subtropical continents the circumstances favor a rather strong warming due to a restricted latent heat flux feedback (because of very low soilmoisture). Furthermore in these regions the models tends to advect water vapor from oceanic or wet land regions into these dry areas.

One may assume that in most regions the land-sea contrast is caused by local differences in the amplitude of latent heat flux. The increase of evaporation over land upon warming is limited, reducing the relative humidity in the boundary layer over land, and hence also enhancing the land/sea contrast. The non-linearity of the Clausius-Clapeyron relationship of saturation specific humidity to temperature is critical. However, when latent heat, which is stored in atmospheric water vapor, is transported by the atmospheric circulation from oceanic to land regions, this amplifies the warming over land (see section 5.2.2).

A far too strong warming is located in the region of the antarctic shelf ice region, whereas the warming over the Antarctic continent is significantly smaller than that proposed by IPCC. This is suggesting that the configured simple climate model is missing some important physics that control the warming response in that region (see section 5.2.3).

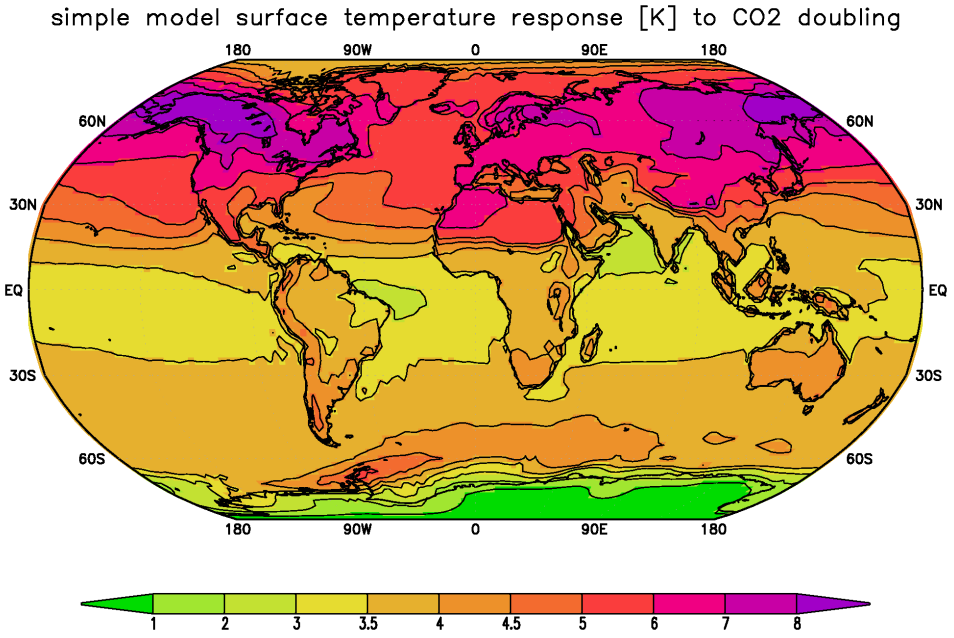


**fig.5.1.** Equilibrium surface temperature response of the simple climate model to CO2 doubling. All processes are included. $\alpha_{ice} = 0.6$.

Since the surface temperature is coupled to the atmospheric temperature by sensible and latent heat flux, the atmospheric temperature should evolve in a somewhat similar way to the surface temperature. In figure 5.2 the anual mean response pattern for the atmospheric temperature to $CO_2$ doubling is illustrated. One clearly see the similarities to figure 5.1 of the surface temperature. Since the atmospheric layer is not differing between land and ocean and additionally is influenced by horizontal advection and diffusion, the pattern does not show locally strong gradients in temperature change.

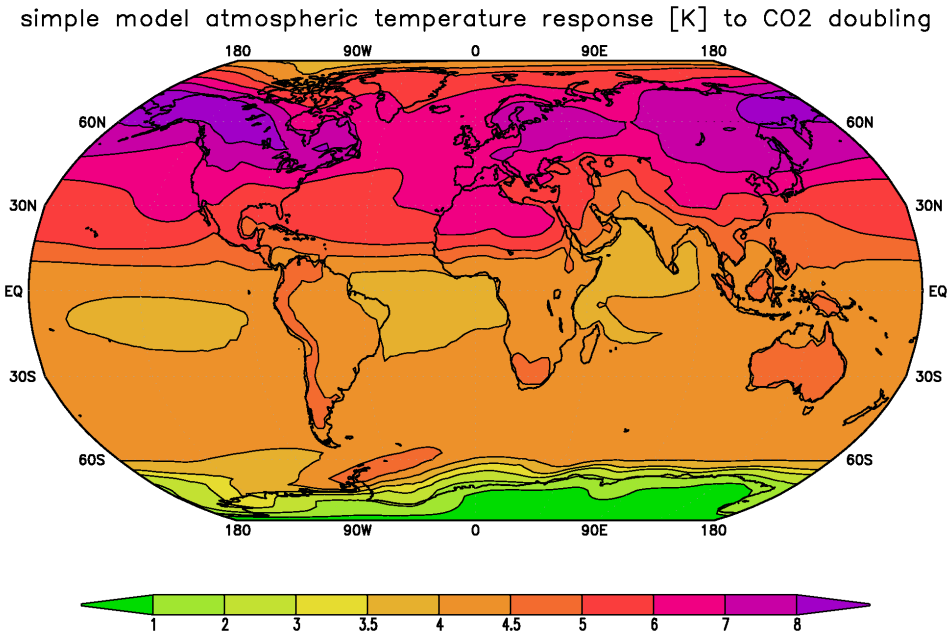


**fig.5.2.** Response pattern for the atmospheric temperature to $CO_2$doubling. All processes, including the albedo feedback, were included.

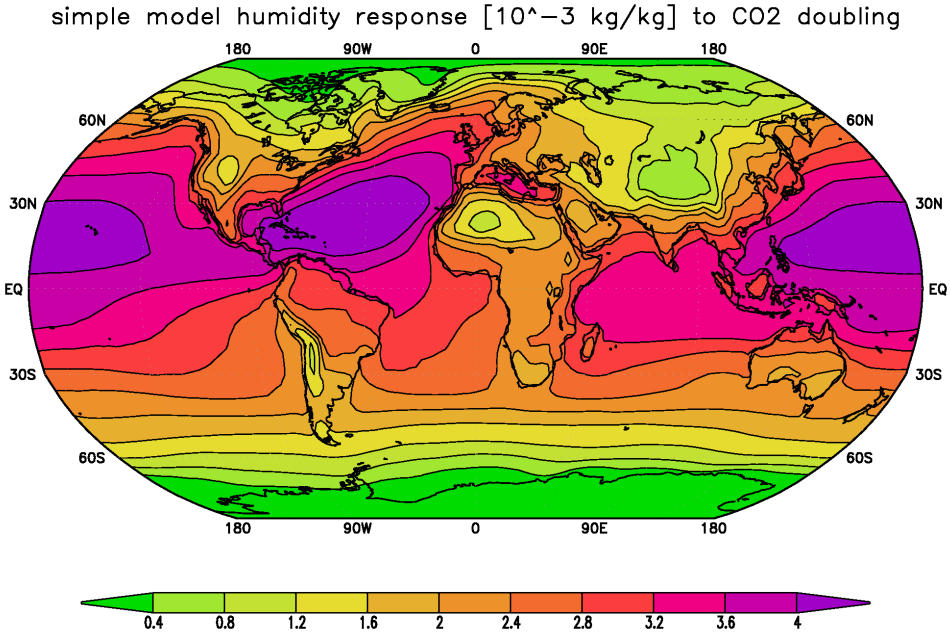


**fig.5.3.** Annual mean response of atmospheric specific humidity to $CO_2$doubling. All processes were included.

The third central variable in the model is the atmospheric specific humidity. Its response pattern to a $CO_2$doubling is shown in figure 5.3. On a global average atmospheric humidity is increasing und global warming conditions, a feature which explained by the positive water vapor feedback (see section 5.2.2). Strongest humidity increases of up to $+4 \bullet 10^{-3} \frac{kg}{kg}$ occur over the tropical and subtropical oceans. However, a significant shift to the northern hemisphere is present. Due to atmospheric transport the humidity anomalies are advected to higher latitudes and also on land regions. The minimal humidity changes in polar regions on both hemispheres show the same pattern as can be seen in the surface temperature change pattern. This implies, that due to missing additional water vapor in these regions the water vapor feedback is not able to amplify the surface warming.

### 5.1.2 Seasonal variation of the global warming response patterns

Since most feedback mechanisms vary in amplitude over the year the surface warming pattern will certainly show seasonal differences as indicated in section 1.1. Since the dominant seasonal variation is introduced ba the solar insolation and local snow cover in middle and high latitudes, the strength of the ice-albedo feedback will strongly vary between summer and winter. According to IPCC AR4 the common characteristics of sea ice change are a peak surface warming in autumn and early winter. The actual snow reductions are greatest in spring and late autumn/early winter, indicating a shortened snow cover season.

In order to illustrate the seasonal variaiton of the model response pattern for surface temperature two three-months mean reonse patterns for winter (DJF) and summer (JJA) are shown in figure 5.4. According to the seasonal variation of ice and snow cover the potential for the ice-albedo feedback to alter the temperature response to a global warming scenario is higher in winter than in summer because of the greater ice cover in the cold season. Thus in boreal winter (DJF) the surface temperature change is strongest on the northern hemisphere reaching values of up to +12K which is roughly 4K more than in the annual mean response pattern. Over the southern hemisphere the winter temperature change pattern shows deviations from the annual mean response in the Antarctic shelf region, which implies a missing ice-albedo feedback being active. On the other hand, in the summer (JJA) temperature change pattern the alues over the northern hemisphere are strongly reduced. This is caused by a missing albedo feedback since no widely spread ice or snow cover is present in this season. Now the water vapor feedback is dominating the response pattern of the northern hemisphere which is causing maximum values of temperature increase of +7K, which is less than in the annual mean case. Over the southern hemisphere a quite distinct pattern at the ice edge of the Antarctic shelf ice region is seen. This is caused be the ice-albedo feedback. In the annual mean pattern this effect is still visible but reduced due to time averaging over all seasons throughout the year.

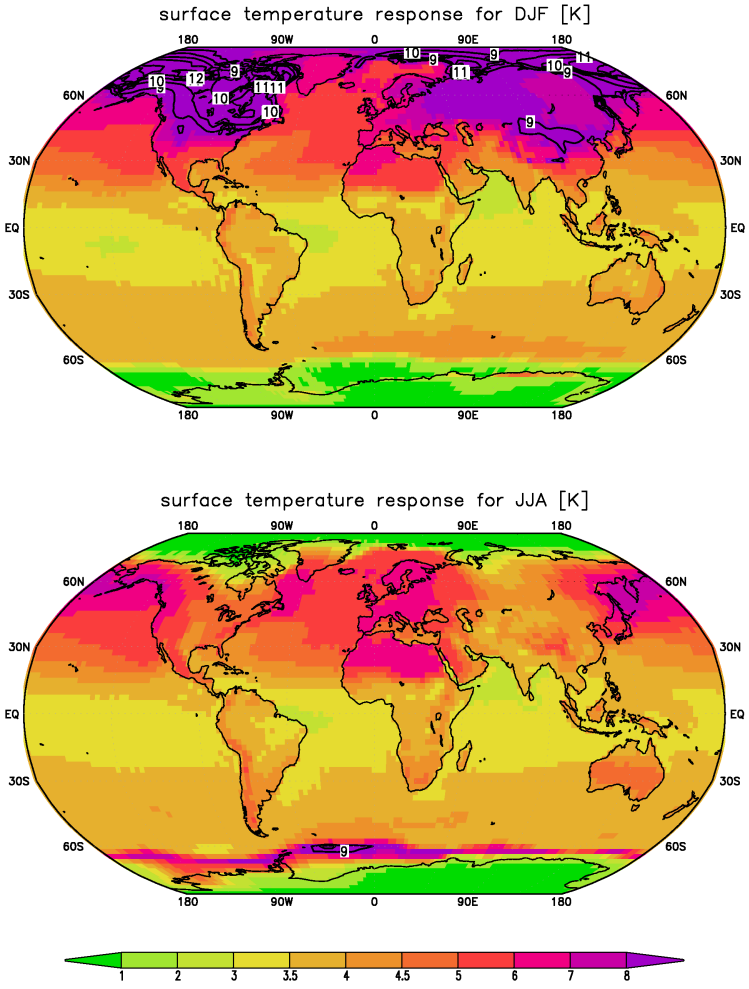


**fig.5.4.** Seasonal response patterns for the surface temperature in winter (DJF, top) and summer (JJA, bottom).

## 5.2 Feedback experiments

Several combinations of feedback mechanisms were used to distinguish the different effects from single feedback processes. See table 5.1 for the experimental setups. For each model experiment the control run (CO2=340ppm) was integrated for 5 years and the global warmig scenario (CO2=680ppm) was integrated for 20 years in order to achieve an equilibrium climate. The difference between both equilibium model climate states are shown in the following subsections. The global average equilibrium temperature difference of the earth´s surface (K) is given in table 5.1.

| | LW | $Q_{sens}$ | $Q_{lat}$ | circ(T) | circ(q) | $\Delta q_{lat}$ | FC | $\Delta\alpha$ | $\Delta T$ |
|---|---|---|---|---|---|---|---|---|---|
| 1 | x | | | | | | x | 0 | +1.10 K |
| 2 | x | x | | | | | x | 0 | +0.96 K |
| 3 | x | | | | | x | x | 0 | +3.18 K |
| 4 | x | | x | | | x | x | 0 | +0.41 K |
| 5 | x | x | x | | | x | x | 0 | +2.81 K |
| 6 | x | x | x | x | | x | x | 0 | +2.64 K |
| 7 | x | x | x | | x | x | x | 0 | +2.22 K |
| 8 | x | x | x | x | x | x | x | 0 | +2.41 K |
| 9 | x | x | x | x | x | x | x | 0.3 | +4.27 K |

**tab.5.1** Experimental setups for studying feedback effects. The processes included in the specific model version are marked with a cross and the albedo difference between ice/snow-covered regions and ice-free regions is given in the last column.

By comparing the given values for the global mean temperature increases for the various model experiments, one can clearly distinguish between the feedback mechanisms either acting positively or negatively on the overall response. The dominant positive feedback processes are the water vapor feedback and the ice-albedo feedback, whereas the latent heat flux acts as a negative feedback. In the following the specific response patterns are discussed. A first result is that overall, the sum of all additional feedbacks is acting as a positve feedback and thus amplifying the surface temperature change on the global average.

### 5.2.1 Longwave radiation feedback and coupling to the atmosphere

The fundamental feedback mechanism controlling the global surface warming pattern is the longwave radiation emitted from the surface and partially re-emitted by the atmosphere, the latter being the so-called greenhouse effect. Since this energy flux directly depends on temperature it plays the central role in determining the temperature change induced by external forcing. In figure 5.5 the annual mean surface temperature response to a doubling in atmospheric $CO_2$ concentration is illustrated. Under the assumption that the local greenhouse effect is proportional to the ground temperature the positive longwave radiation feedback is strongest in regions with relatively high surface temperatures. Thus to first order this pattern reflects the annual mean surface temperature field of the earth (see figure 4.6). The strongest warming is located in the tropics with amplitudes up to +1.4K, whereas the temperature change is decreasing poleward and reaching values of less than +0.6K in both hemispheres polar regions as well as in high altitude regions such as the Rocky Mountains, the Andes and the Himalayas. Thus the major effect of the longwave radiation feedback, if acting as a single process, is strengthening the equator-to-pole temperature gradient, which then may induce dynamical changes within the atmospheric circulation pattern. This feedback, however, is not implemented into this model. On a global average the surface temperature increases by +1.10K. The pattern shows a land-sea contrast and local gradients in temperature change, since in general the surface temperature is controlled by a latitudinally varying solar forcing and the elevation of the surface, showing lower temperatures and thus lower temperature responses over high continental plateaus (e.g., Tibet) or ice shelfs (e.g., central Greenland or Antarctica). However, the land-sea contrast (with stronger warming over land), which is seen in observations and common GCM results for global warming scenarios is not present in this pattern. It only appears when local feedbacks and lateral energy fluxes are included into the system.

Then the reponse is altered and thus shows local features controlled by certain characteristics, such as, surface albedo, soilmoisture etc. These effects are discussed in the following subsections.

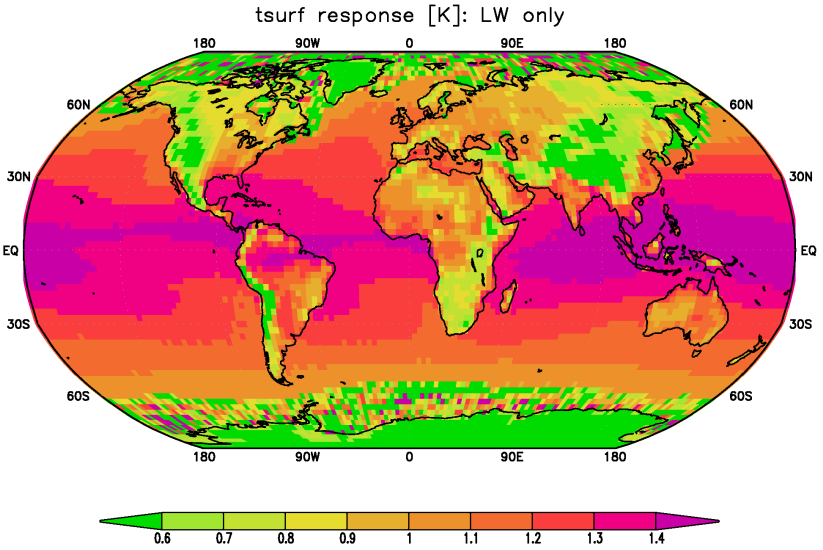


**fig.5.5** Surface temperature response to $CO_2$ doubling. Only the longwave radiation feedback is active. Difference is taken between a 340ppm control run and a 680ppm scenario run, which both were run into equilibrium.

In the following, the sensible heat flux will be discussed shortly. Indeed, the sensible heat flux is just implemented into the model in order to couple the surface temperature to that of the atmosphere. Since the atmospheric layer is somehow artificial, this process has rather a functional than a physical character, because to represent the sensible heat flux in a sufficient way one would need the 'real' atmospheric boundary layer temperature. This is not possible in this conceptual model and hence the only way sensible heat is affecting the surface temperature is by projecting the atmospheric temperature pattern down onto the surface. In doing so, the atmospheric processes of horizontal advection of temperature and humidity and latent heat release are resolved. Considering all this, one should expect the surface response pattern to remain unchanged when sensible heat flux is included whereas atmospheric trasnport and latent heat flux are neglected. Just for clarifying this model feature, the difference between the surface response patterns with and without sensible heat flux is shown in figure 5.6 below. The temperature differences can be taken as being within the range of the model's computational accuracy with values mostly below $\pm 0.01K$. Only in sea ice regions the effect of sensible heat results in temperature differences up to $\pm$0.1K.

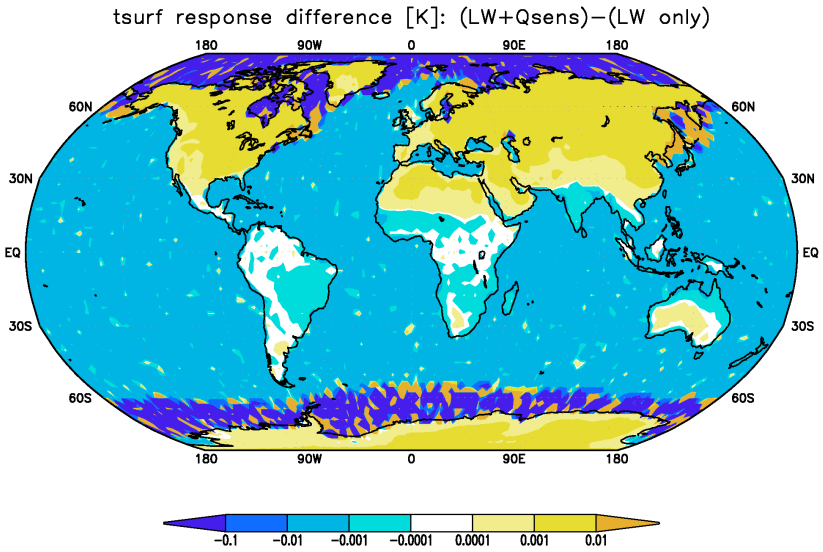


**fig.5.6** Difference in surface temperature change due to $CO_2$ doubling between a model setup only consisting of longwave radiation and another setup which also includes sensible heat flux.

### 5.2.2 Hydrological cycle feedbacks: water vapor and latent heat flux

So far only the net longwave radiation at the surface and the sensible heat flux between surface and atmosphere were considered. Now the components of the hydrological cycle are included, which are:

- water is evaporated at the surface and introduced into the atmosphere
- latent heat flux is lost by the surface and released within the atmospheric layer
- both atmospheric humdity and latent heat are horizontally distributed within the atmosphere

In the following, the effects of single components of the hydrological cycle on the model's response pattern will be discussed. For an overview over the experimental setups, see the table in the beginning of this section.

For the first experiments atmospheric transport is neglected. In a simple model setup for the water vapor feedback besides the longwave radiation feedback the atmospheric water vapor concentration is allowed to vary seasonally and is altered by evaporation at the surface. Precipitation rates are assumed to only depend on the local water vapor amount and the mean residence time of water vapor, which is roughly ten days. The resulting surface temperature response pattern for this model experiment is shown in figure 5.7 (top). In comparison to figure 5.5 an additional water vapor feedback is introduced. Since this feedback is positive it will amplify the temperature response in those regions that experience an increase in atmospheric humidity. Thus a strong amplification of the greenhouse effect is taking places due to higher water vapor absorption and emission of longwave radiation. Thus the surface long wave radiation loss is strongly reduced, causing higher temperature increases. This is the case in all regions except of the continental ice sheets of Greenland

and Antarctica, where due to very low evaporation the humidity stays at quite low values and therefore does not provide an response amplification due to the water vapor feedback. In all other regions the atmospheric humidity is increased by additional evaporation of water from the surface. Especially over the subtropical oceans the increased water vapor concentration leads to temperature changes up to +5K, which is roughly a triplication of the values that would result from neglecting this positive feedback (compare with figure 5.5). In middle and high latitudes the amplification only accounts for an amplification of additional +1 to +2K, which roughly is a doubling of response. Over the polar regions the watervapor feedback is nearly negligible. Thus including the water vapor feedback into the system will strengthen the equator-to-pole temperature gradient.

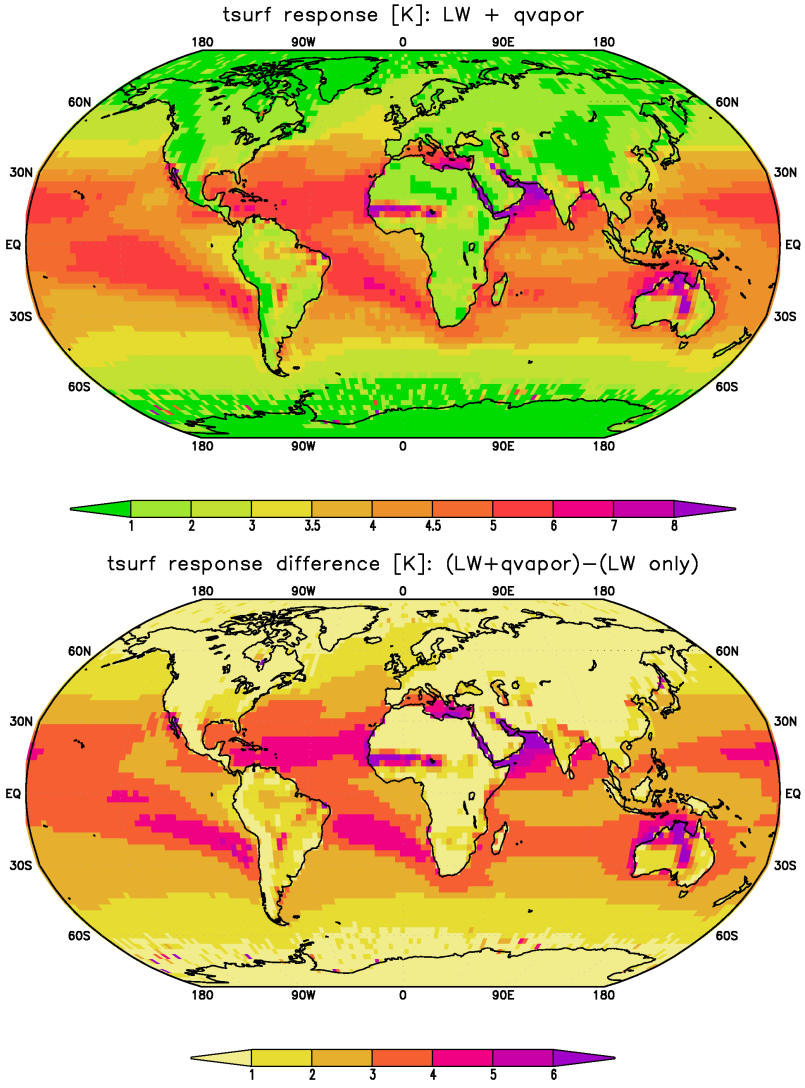


**fig.5.7** (top) Surface temperature response according to $CO_2$ doubling when only the longwave radiation feedback is active and atmospheric humidity is allowed to vary according to evaporation and precipitation. (bottom) Response difference between the model versions with and without water vapor response. Thus the pattern illustrates the effect of the water vapor feedback just resulting from humidity variations.

Without lateral diffusion and advection there is a quite distinctive land-sea contrast with a stronger warming over the oceans than over land. Obviousy, this results from the higher moisture availability in oceanic regions, whereas in relatively dry land regions the potential evaporation is limited.

The absolute change in specific humidity at the surface which is accompanying this temperature response pattern is shown in figure 5.8 below. There it is clearly visible that humidity strongly increases in regions with high energy input at the surface,such as in the tropics, and where soilmoisture is large (e.g., over the oceans and wet land areas). There maximal increases of up to $6 \bullet 10^{-3} \frac{kg}{kg}$ occur, whereas in polar regions and over very dry or high altitude land regions no significant change in atmsopheric humidity takes place. Obviously, when no lateral atmospheric transport of humidity takes place, on average a stronger warming would occur over the oceans due to stronger incraese in water vapor and thus a stronger amplification of the local greenhouse effect. On a zonal average the humidity increase is stronger over the southern than over the northern hemisphere. This of course is to a first order a result of the heterogenic land-sea-distribution among both hemispheres with the southern hemisphere consisting of more oceanic regions than land masses.

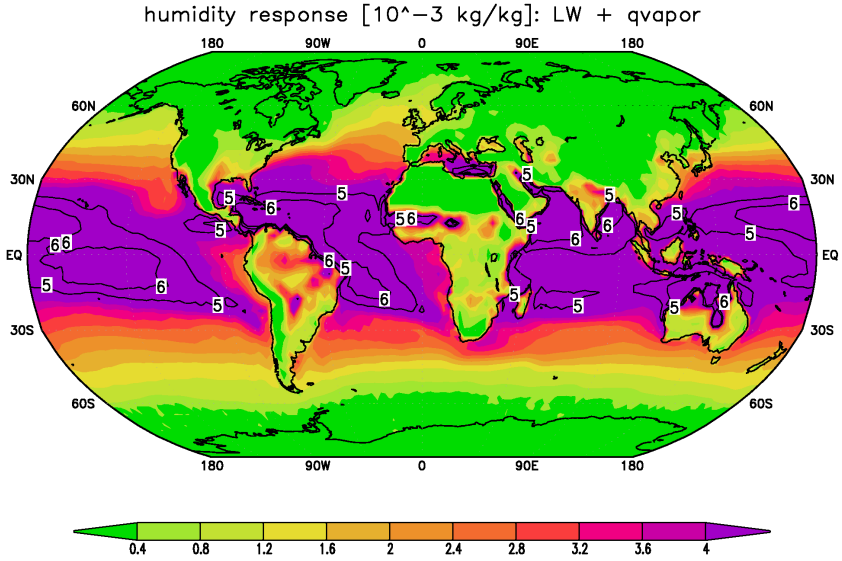


**fig.5.8** Surface specific humidity change due to $CO_2$ doubling. Units are $10^{-3} \frac{kg}{kg}$. Only longwave radiation and water vapor feedback are active.

Certainly, this experimental model setup does not represent a realistic scenario, since a second important process, which is the latent heat flux from the surface to the atmosphere, is neglected. This mechanisms is generally acting as a negative feedback and thus dampens the expected temperature response. For a sufficient representation of the latent heat feedback it is necessary to include the atmospheric branch of the model. Thus a certain amount of the latent heat flux entering the atmosphere is released in accordance with condensation processes and therefore locally increasing the atmospheric temperature. This signal will then be given back to the surface via the sensible heat flux, which couples the surface to the atmosphere. Thus now the positive water vapor feedback together with the negative latent heat flux feedback are competing and this way compensating each other to a certain level. If one sets up a model experiment with longwave radiation, water vapor feedback and additionally sensible and latent heat flux affecting the surface, the temperature response would change in a way as illustrated in figure 5.9 below. The initial warming (resulting from

longwave radiation and water vapor feedback only) is strongly dampened over tropical and subtropical oceans and some wet land regions since the latent heat flux feedback is strongly negative due to increased heat loss as surface temperatures increase. Over the tropical and subtropical oceans, where the potential latent heat flux is very high due to high sea surface temperatures and, specificly in the subtropics, a quite low relative humidity in the atmosphere, the temperature response is reduced by up to 0.5K, which is a reduction by about 10% of the initial value resulting from the water vapor feedback. Over the mid- and high-latitude oceans and most land surface regions the reduction in temperature response is only slightly reduced because latent heat fluxes are small. In these regions the latent heat flux is reduced as a result of lower temperatures (meaning a lower saturation specific humidity) and higher relative humidity. Thus the magnitude of the negative feedback is reduced. An only negligible effect of the latent heat feedback is seen over regions with extremely low soilmoisture (e.g., Sahara, Greenland and Antarctica) where there is almost no potential latent heat flux. Overall, the similarity between the latent heat reponse pattern and the change in water vapor is obvious, since the water vapor flux is taken to be proportional to the latent heat flux.

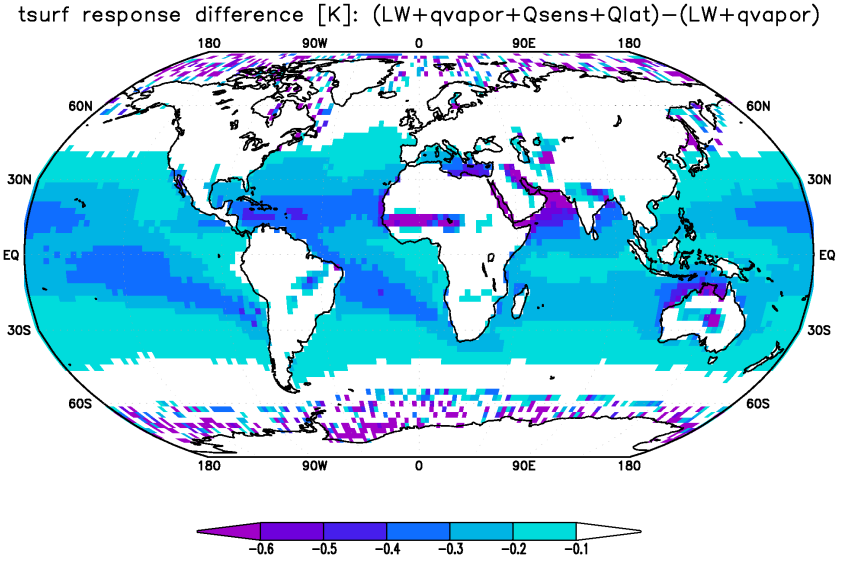


**fig.5.9** Difference in surface temperature response between two model setups: 1) longwave radiation, latent heat flux and sensible heat flux and 2) longwave radiation, latent heat flux, but no sensible heat flux.

Now if together with the vertical components of the hydrological cycle the horizontal transport of sensible and latent heat within the atmospheric layer are integrated into the model, the response pattern is changed significantly according to the advection pattern and lateral diffusion. At first, only the horizontal transport of sensible heat is included, leading to the response pattern shown in figure 5.10 (top) below. Obviously the major effect of lateral temperature advection and diffusion is to smoothen the local gradients in the response pattern and to transport heat from low to high latitudes on both hemispheres. This effect is shown more clearly on figure 5.10 (bottom), showing the diefference betwenn the model setups with and without atmospheric transport of heat. The most striking effect is the enhancement of temperature increase over land by up to about 1.5K and a dampening of response over the oceans by up to 2K.

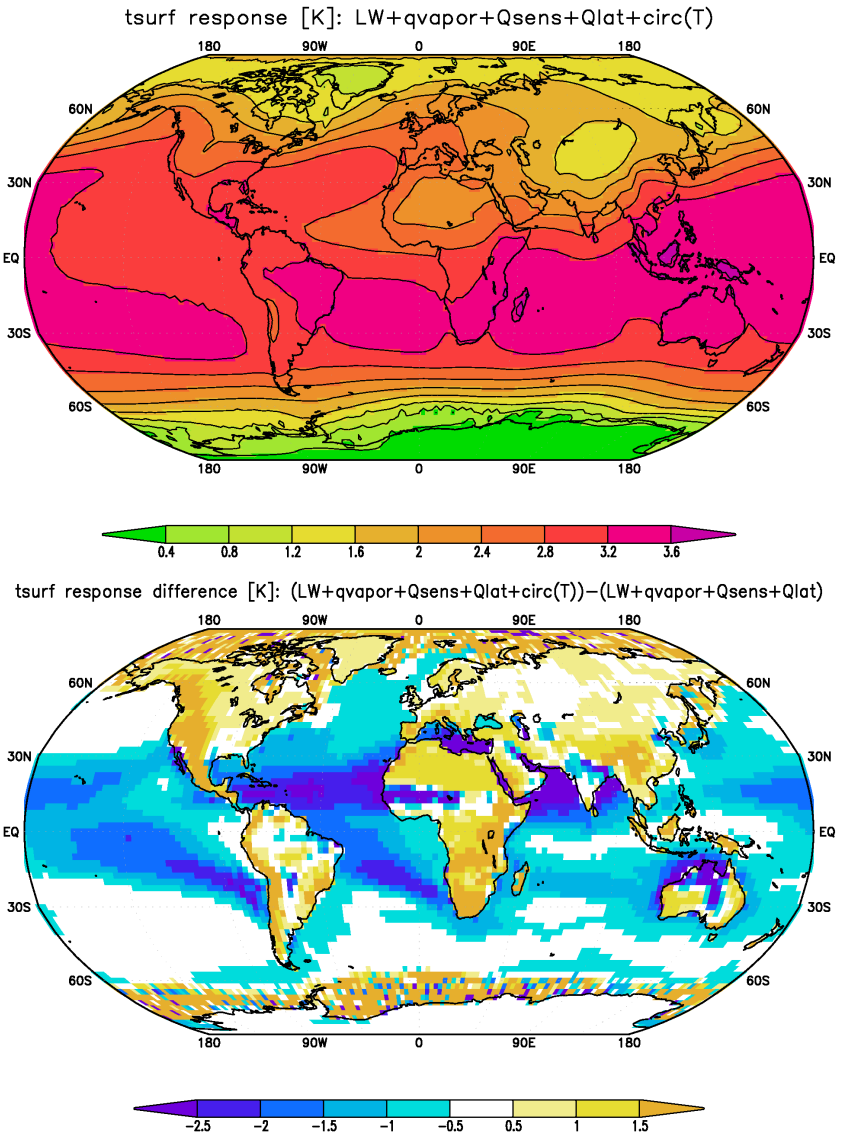


**fig.5.10** (top) Surface temperature response to $CO_2$ doubling with the surface radiation balance, the vertical components of the hydrological cycle (water vapor flux, latent and sensible heat fluxes) and the atmospheric transport of temperature by advection and diffusion. (bottom) Corresponding response difference between the model setups with and without atmospheric transport of temperature.

In order to estimate the contribution of atmospheric humidity transport by advection and diffusion an experimental model setup without temperature diffusion was integrated, resulting in the pattern shown in figure 5.11 (top). From this result it is clearly visible that most of the amplified warming over land comes from the net transport of atmospheric humidity from the oceans to land, which reduces the net effect of the water vapor feedback over the oceans while increasing it over land. Thus a distinct land-sea contrast is introduced into the global surface warming pattern resulting from increasing $CO_2$ concentration. To visualize this effect more clearly the difference pattern from the just described

experiment to the corresponding model setup with no atmospheric humidity transport is shown in figure 5.11 (bottom). Very strong gradients in temperature change occur at the edges of the continents, where moisture transport from ocean to land is enhancing the local greenhouse effect. Of course this mainly occurs on the western boundary of the continental areas laying in the mid-latitude west wind zone. This feature is also seen over land where regions with strong evaporation are bordering to very dry regions. Here the dry regions gain additional atmospheric water vapor due to atmospheric transport and thus experience an enhanced warming, whereas in the region where the water vapor originates from the warming is dampened. This can be seen over the Saharan desert or the Tibetan Plateau, whereas over tropical Africa the warming amplitude is decreased since water vapor is on average transported out of this region.

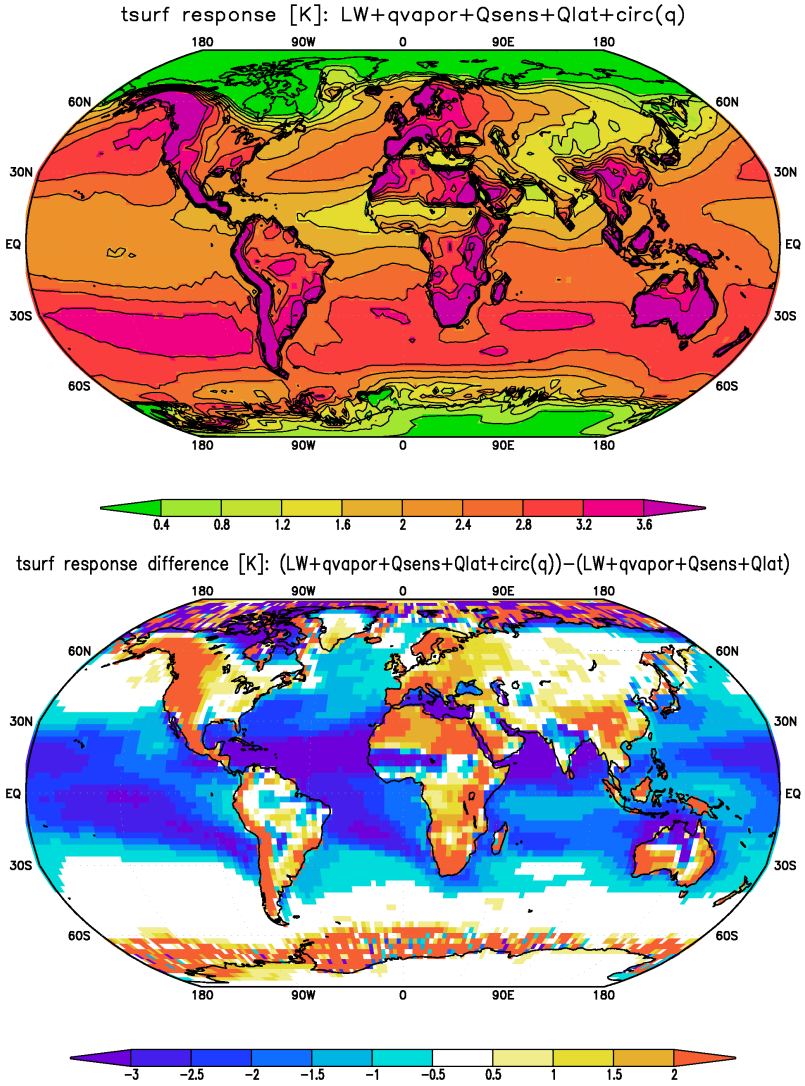


**fig.5.11** (top) Surface temperature reponse to $CO_2$ doubling including longwave radiation, latent heat flux, sensible heat flux, variable water vapor and lateral diffusion of humidity. (bottom) Difference pattern of the response pattern above to that without atmospheric heat transport.

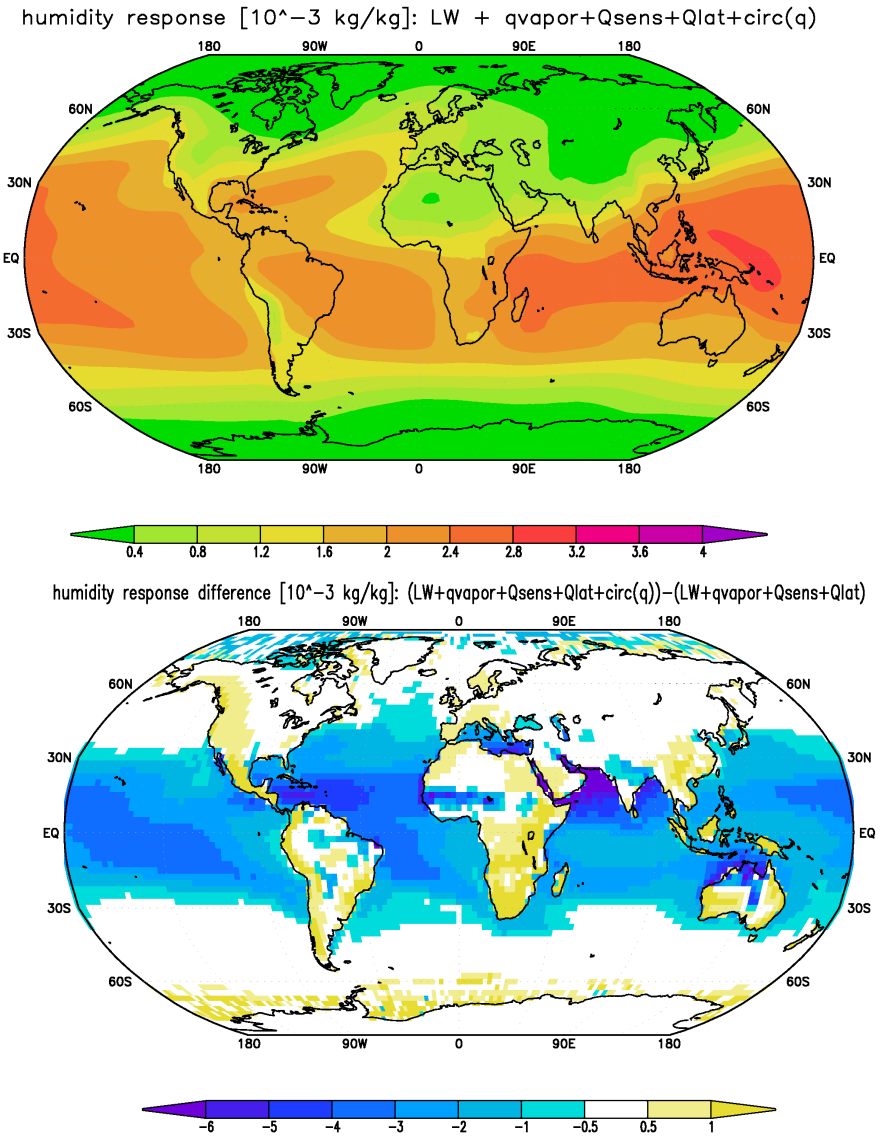


**fig.5.12** (top) Change in specific humidity to $CO_2$ doubling resulting from a model experiment that consists of longwave radiation, sensible heat flux, latent heat flux, variable water vapor and atmsospheric transport (advection and diffusion) of humidity. (bottom) Response difference to a corresponding model version with no atmospheric humidity transport.

The corresponding changes in atmospheric humidity that is resulting from a model setup including atmospheric humidity transport can be seen in figure 5.12 (top). In addition the response difference between the model versions with and without atmospheric transport of humidity is shown (bottom). Due to the redistribution of the water vapor from regions with high evaporation rates to regions with lower atmospheric humidity strongly decreases the maximum change in humidity which is now around $+3 \bullet 10^{-3} \frac{kg}{kg}$. Highest humidity response still lies in the tropics and subtropics but now shows no significant gradients between ocean and land regions. Towards the polar regions the humidity response decreases to

values around $+0.4 \bullet 10^{-3} \frac{kg}{kg}$. As one sees in the corresponding difference pattern, the largest changes in the humidity response due to amospheric trasnport occur in low and middle latitudes where originally the evaporation rates show the largest contrasts between ocean and land. The similarities between the humidity and temperature difference patterns caused by atmospherix moisture transport are obvious, since the local convergence of atmospheric water vapor induces a stronger local greenhouse effect.

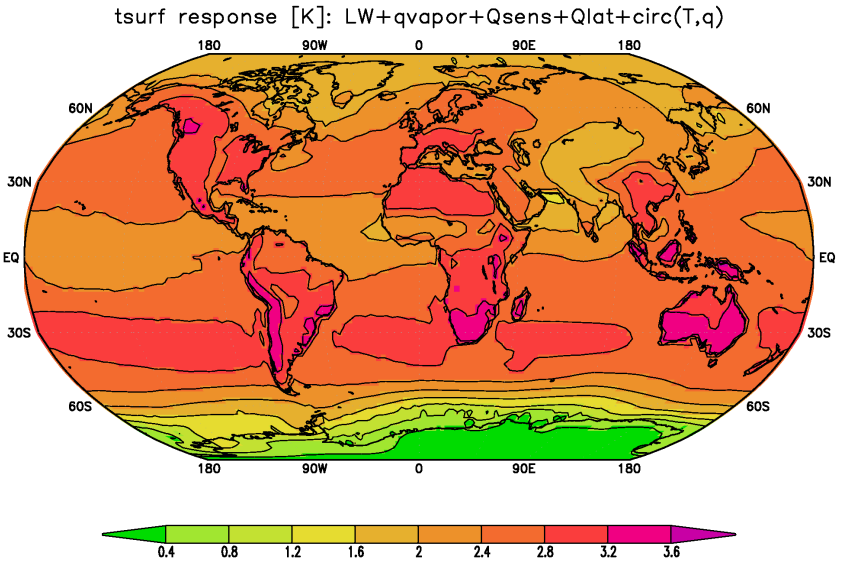


**fig.5.13** Surface temperature equilibrium response pattern for a doubling of atmospheric CO2 concentration when next to longwave radiation the complete hydrological cycle is included: latent heat flux, sensible heat flux, variable water vapor, lateral diffusion of temperature and humidity.

In order to show the complete response due to the hydrological cycle there are now all processes included: longwave radiation, sensible heat flux, latent heat flux, variable atmospheric water vapor and atmospheric transport of atmospheric temperature and humidity. The overall response pattern is shown in figure 5.13. One clearly sees a quite significant land-sea contrast with stronger warming over land and regionally less warming over the ocean. The highest temperature increases of around +3.4K are seen in mid-latitude land regions on the southern hemisphere. These are caused by strong humidity increases over the oceans, which make up most of the southern hemisphere and thus provide more water vapor, and advection of this moisture onto the land regions. Of course, a similar feature is present on the northern hemisphere where strong moisture convergence over the western parts of the mid-latitude continents (eastern North America and western Europe) induces an amplified warming of up to +3K. A local minimum of around +2K within the latitudinal variation of this temperature response pattern occurs in the tropics where indeed local evaporation is high, inducing a positve feedback, but local atmospheric transport leads do a net humidity divergence and thus a reduction in the potential water vapor feedback. The lowest temperature response values occur in the polar regions, where the water vapor feedback is low and atmospheric transport does not favour a sufficient moisture convergence. Since the great continental ice sheets are assumed to vary on timescales longer than those playing a role for typical global warming scenarios, the continetal ice-coverage of Greenland and Antarctica are held constant in the model and are therefore not able to respond to the ice-albedo feedback. In Arctic regions the temperature only increases by around 1.6-2K

whereas in the Antarctic regions only values of +0.4 to +1.6K are found. Due to the strong circumpolar west wind drift surrounding the Antarctic continent isolate this part of the earth surface from the warming trends elsewhere.

If one now compares the last temperature response pattern with that of the first experiment with only longwave radiation, then the first thing to notice is that the combination of water vapor and latent heat feedback overall gives an amplification of the temperature response pattern in comparison to the longwave radiation response. On a global average the surface temperature increases from +1.10K to +2.41K, which roughly is a doubling in sensitivity in comparison to the longwave radiation response. Due to the atmospheric transport the strongly positive water vapor feedback is spread not only in regions where high water vapor fluxes from the surface into the atmosphere occur but also in regions with minor evaporation but positive moisture convergence in the atmosphere. In general the land surface warm more than the oceans, especially in the subtropics and mid-latitudes. Minimal temperature changes around +1K still occur over the Antarctic continent.

### 5.2.3 Ice-Albedo-Feedback

In the following section the ice-albedo feedback will be discussed. Whereas the previously illustrated water vapor feedback is altering the temperature response to $CO_2$ doubling nearly all over the earth surface, the ice-albedo feedback is spatially restricted to those regions where a change in ice or snow coverage takes place during the seasonal cycle. This is the case over land as well as over the oceans in high latitude regions on both hemispheres. If a decrease in surface albedo is allowed in correspondence to rising temperatures and according melting processes in ice-covered regions, the positive ice-albedo feedback is amplifying the temperature response in those regions where as net change from ice-covered to ice-free areas occurs. Thus a larger amount of solar radiation (due to smaller surface albedo) is absorbed by the ground, which then is balanced by an increased emission of long wave radiation due to higher temperatures. The surface temperature response pattern resulting from all processes included in the model (longwave radiation, sensible and latent heat fluxes, varaible water vapor, atmospheric heat and humidity transport and the ice-albedo feedback) is shown in figure 5.14 (top) together with the response difference pattern with a model version without the ice-albedo feedback being active (bottom). Due to the ice-albedo feedback the temperature response in middle and high latitudes of the northern hemisphere reaches maximum values up to +8K, whereas in the shelf region of Antarctica temperature changes of up to +4-5K occur. Of course this pattern includes the smoothening effect of atmospheric heat transport. The strong Antarctic Circumpolar Current (ACC) and the corresponding West Wind Drift in the atmosphere are strongly isolating the Antarctic Continent from the rest of the climate system. Thus sea ice melting should be reduced in this region, which would dampen this strong warming. Thus the amplifying potential of the positive ice-albedo feedback in the Antarctic region is masked by the strong advection in this region where temperature anomalies are widely distributed in zonal direction and also towards lower latitudes. Thus the surface temperature response is weaker than on the northern hemisphere where local wind velocities are smaller and not that homogenous. In the Arctic region the redistribution of the temperature anomalies induced by the ice-albedo feedback is governed by local wind field which may alter in direction and amplitude among different regions. Thus the strong temperature signal orginating from the seasonal ice edge is spread polwards as well as equatorwards. The local minimum of the response pattern of the inner Arctic is caused by the net divergence of the wind field within that region that prevents the positive temperature anomalies to propagate into that region and cause a further feedback effect. Over northern Canada, for instance, the annual mean winds have a strong southward component, causing advection of relatively dry and cold air and thus

dampen the ice-albedo feedback. Overall the ice-albedo feedback is strongly amplifying the global surface temperature response to $CO_2$ doubling with a global average temperature increase by +4.27K. Thus in comparison to the model response without ice-albedo feedback the temperature response is amplified by additional +1.86K. As can be seen in the response difference pattern (figure 5.14, bottom), the warming effect resulting from the albedo feedback at the ice edges is spread over the whole globe by atmospheric heat transport. Thus even the waming response in the tropics is amplified by at least +0.5K.

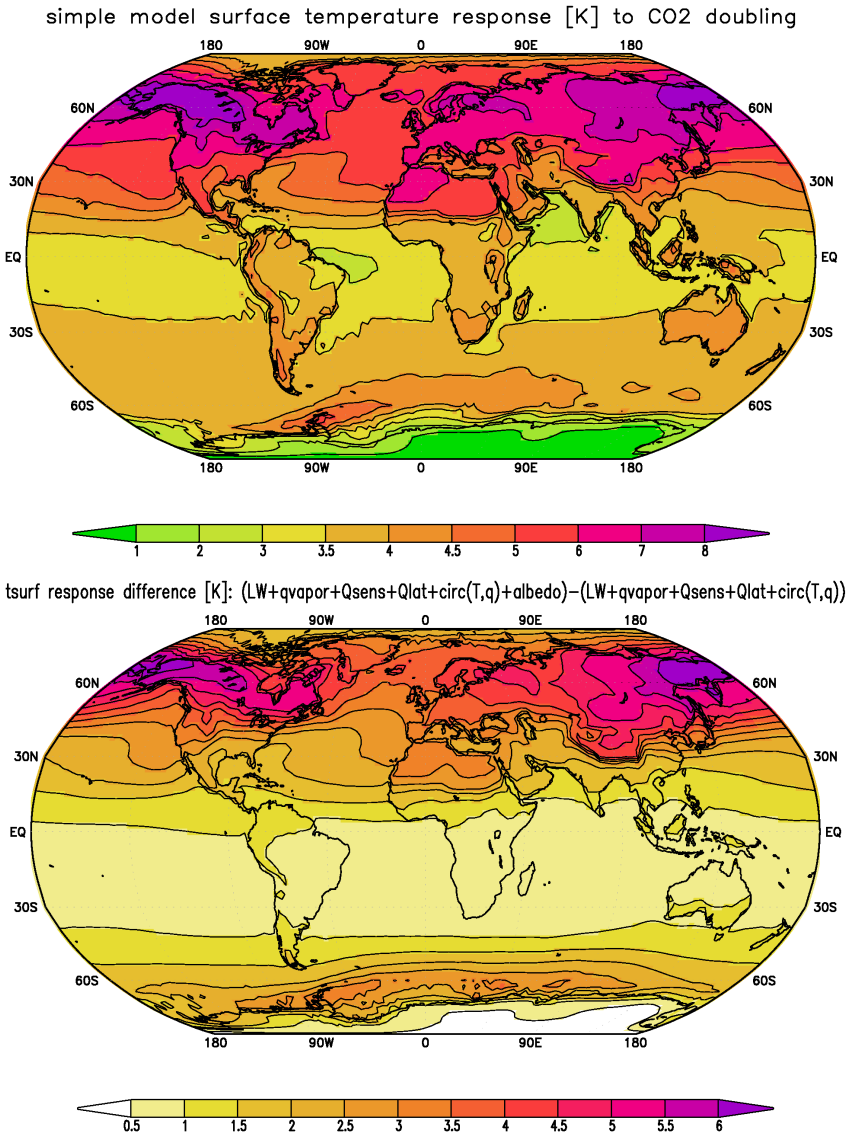


**fig.5.14** (top) Equilibrium surface temperature response of the simple climate model to $CO_2$ doubling. All processes are included: longwave radiation, sensible and latent heat fluxes, variable water vapor, atmospheric trasnport of heat and humidity, albedo change ($\alpha_{ice} = 0.6$). (bottom) Corresponding response difference pattern between the model version with and without the albedo feedback being active.

## 5.3 Climate sensitivity for the A1B scenario

Climate sensitivity is a measure used to characterize the response of the global climate system to a given forcing. It is broadly defined as the equilibrium global mean surface temperature change following a doubling of atmospheric $CO_2$ concentration. Climate sensitivity is largely determined by internal feedback processes that amplify or dampen the influence of radiative forcing on climate. One may distinguish between the 'equilibrium climate sensitivity' and the 'transient sensitivity', whereby the order of the letter is determined by the equilibrium sensitivty and the ocean heat uptake. In general the equilibrium value is greater than the transient one. Additionally, the climate sensitivity depends on the mean state of the climate. The concept of climate sensitivity is useful since many aspects of a climate model scale well with global average temperature (although not necessarily across models).

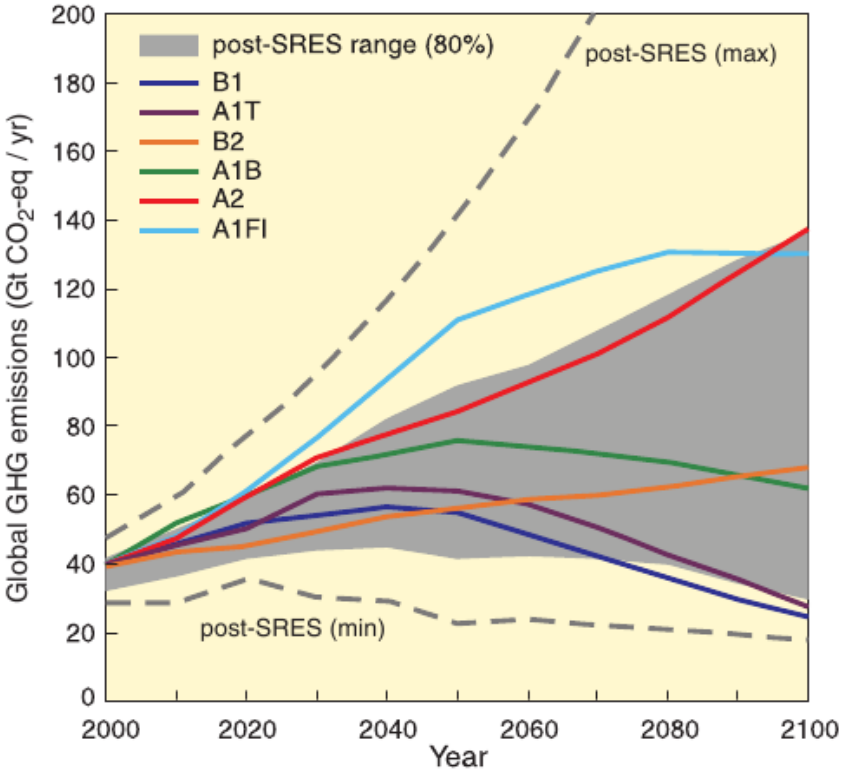


**fig.5.15** Global GHG emissions (in Gt $CO_2$-eq per year) in the absence of additional climate policies: six illustrative SRES marker scenarios (coloured lines) and 80th percentile-erange of recent scenarios published since SRES (post-SRES) (Grey shaded area). Dashed lines show the full range of post-SRES scenarios. The emissions include $CO_2$, $CH_4$, $N_2O$ and F-gases.

On the base of different climate policies and related sustainable development practices (population projections, economic growth, global energy mix, including fossil fuel burning, technological change), several GHG emission scenarios have been estimated for future climate projections and were published in the IPCC Special Report on Emissions Scenarios (SRES, 2000). Post-SRES scenarios have been improved and the correspoding emissions are projected to be lower than reported in SRES. These are shown in figure 5.15, which

is taken from the IPCC-AR4. The corresponding timeseries of atmospheric carbon dioxide concentration is illustrated in 5.16. Typically, the future projections are based upon initial conditions extracted from the end of the simulations of the 20th century. Therefore, the radiative forcing at the beginning of the model projetions should be approximately equal to the radiaitve forcing for present-day concentrations relative to pre-industrial conditions. Among those scenarios, the A1B-scenario represents an intermediate projection, by assuming a world of very rapid economic growth, a global population that peaks in mid-century and rapid introduction of new and more efficient technologies that have a balance across all energy sources (fossil fuels and renewable energies). This scenario will be used for the following calculations.

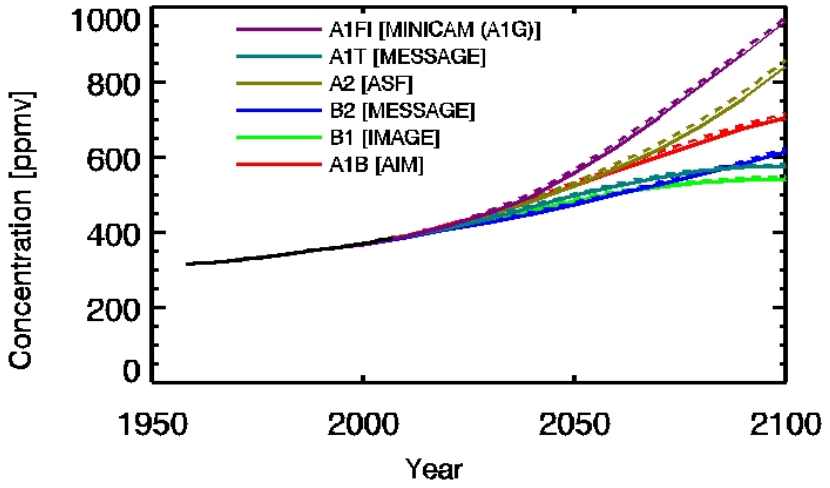


**fig.5.16** Atmospheric $CO_2$ concentrations as observed at Mauna Loa (black line) and projected under the six SRES scenarios. (source: IPCC-AR4)

In the following, the results of the simple climate model are compared with the current IPCC models. The response pattern of the simple climate model to the A1B scenario is illustrated in figure 5.17. The temperature differences were calculated from the equilibrium state ofthe control run, which is supposed to be comparable with the climatology of the years 1950-2000, and the according transient response of the model that corresponds with the time interval 2070-98 of the A1B scenario. In this reponse pattern the two major features of global warming, being the land-sea contrast as well as the polar amplification especially in northern high latitudes, are clearly visible. However, the absolute temperature differences are at least 1-2 times larger than the IPCC projections suggest. For comparison an ensemble mean response pattern of the IPCC models was calculated.

The IPCC models have been integrated to year 2100 following the projected concentrations of long-lived GHGs and emissions of $CO_2$ specified by the A1B emissions scenario. In figure 5.18 you can see the multi-model ensemble mean surface temperature response pattern. The reason to focus on the multi-model mean is that averages across strucutrally different models empirically show better large-scale agreement with observations, because individual model biases tend to cancel. The use of means has the additional advantage or reducing the 'noise' associated with internal or unforced variability in the simulations.

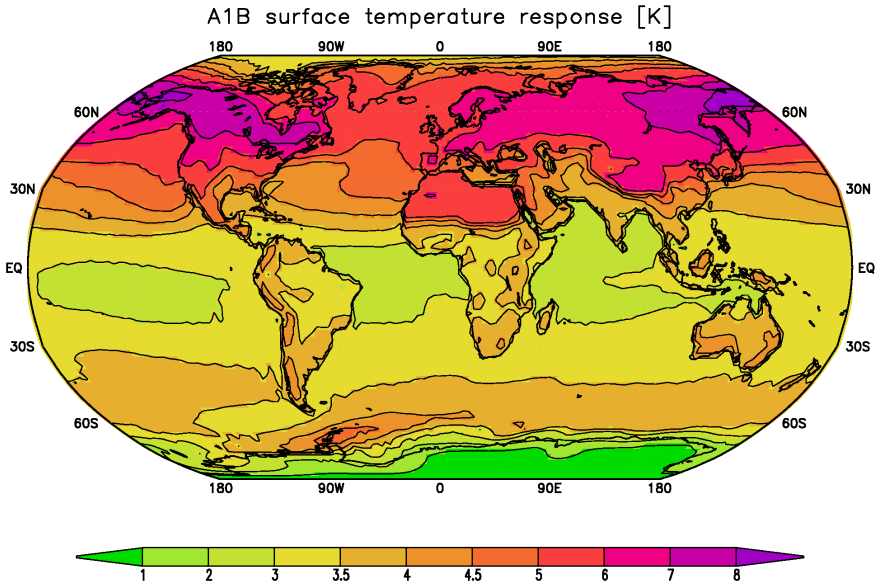


**fig.5.17** Surface temperature response pattern os the simple climate model to $CO_2$ concentration changes according to the A1B scenario.

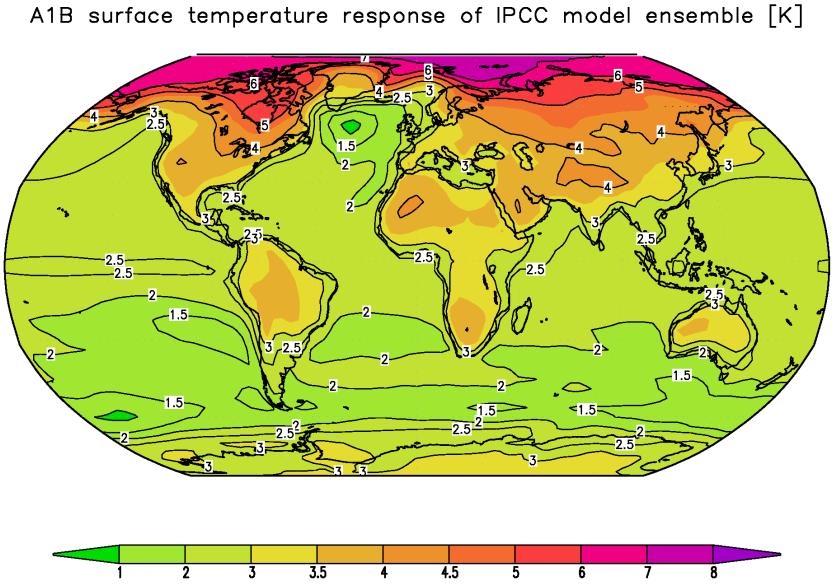


**fig.5.18** Ensemble mean of IPCC model response to the A1B scenario. Surface temperature difference is calculated between the time period of 1950-1999 and 2070-2098.

Now in comparing these two results one clearly sees the similarities in the patterns as well as the differences in the amplitudes. Both results show a strong warming in high northern latitudes with temperature changes of up to +8K in the simple model and up to 7K in the IPCC ensemble, which suggests the sensitivity of the simple model to be too large in comparison to the IPCC models. Further, the strongest warmin in the simple model is not

located over the inner Arctic as in the GCM result. This suggest differences in the sea ice behaviour in that region.

In lower latitudes, the simple model shows temperature increases of around +3K, whereas the ensemble only yields a value around 2.5K, which is again less than the simple model's sensitivity. Nevertheless, the pattern in lower latitudes,including the land-sea contrast, is visible in both results. This suggest that the physics of the simple model indeed lead to the right reponse, but the interactions among the various feedback mechanisms is strongly amplifying the pattern. Thus the strength of the positively acting feedbacks may be overestimated.

In the polar and subpolar region of the southern hemisphere the response patterns differ tremendously. While the IPCC ensemble mean shows a local minimum over the Southern Ocean and temperature changes of +3K in central Antarctica, the simple model reponse is clearly dominated by a strong warming in the region of the edge of the Antarctic sea ice region. There a temperature change of up to +4.5K is obviously caused by an overestimated positive ice-albedo feedback in the simple model. This differences imply that some important physical processes are not given realistically in the simple model.

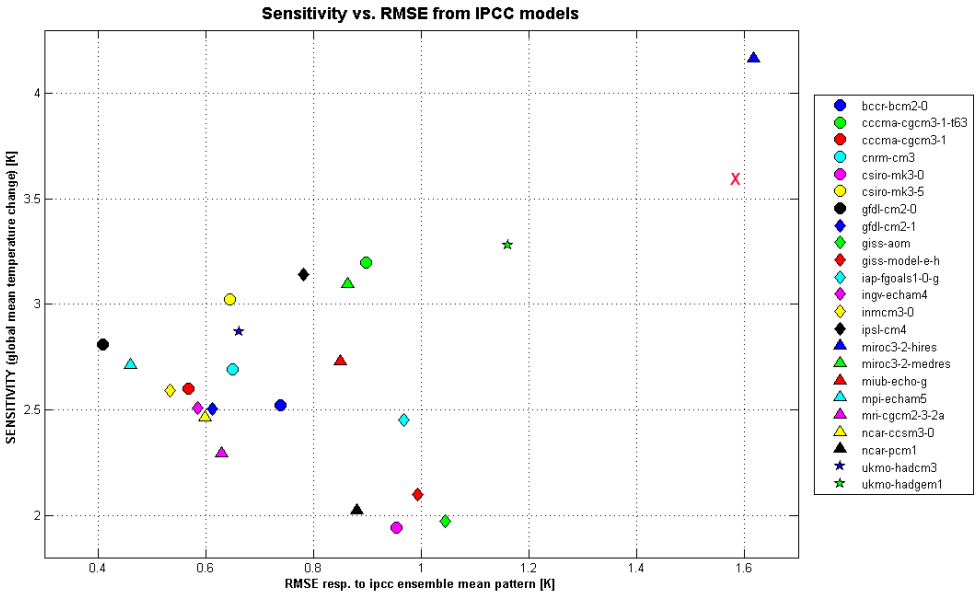


**fig.5.19** The model sensitivity is shown together with the RMS-error of the response pattern from the IPCC ensemble mean pattern. The model sensitivity is calculatecd as the global average surface temperature difference between 1950-1999 and 2070-2098. The values for the simple climate model is marked with a red cross.

In order to quantify the comparison between the simple model result and that of the IPCC ensemble, two metrics were calculated. On the one hand, the sensitivity, which corresponds to the global mean temperature change, is a measure for the amplitude of global warming. On the other hand, a RMS-error has been calculated, which quantifies the deviation of a single model response pattern from the IPCC ensemble pattern (figure 5.18). Both these quantities are shown in figure 5.19 for 23 IPCC models and the simple climate model. All values correspond to the A1B scenario an a temperature difference between the periods 1950-2000 and 2070-2098. For the simple climate model a sensitivity of 3.62K and an RMS-error of 1.59K were determined. Thus in comparison to the IPCC models, the simple

model has both a sensitivity as well as a RMS error that lies within the range of current GCM results for future global warming projections. This agrees with the results from the discussion above.

Because of the nonlinear nature of the response to feedbacks, the final impact on sensitivity is not simply the sum of these responses. The effect of multiple positive feedbacks is that they mutually amplify each other's impact on climate sensitivity. Thus, the sensitivity results of the developed simple climated model strongly suggest that the positive feedbacks (ice-albedo and water vapor feedback) are either overestimated in the model or the role of the negative feedbacks, which would dampen the sensitivity, is to weak. The defficiencies in reproducing the pattern of the surface warmng in all details suggest that more details and further improvements in the sea ice model have to be included into the model.

# Chapter 6

# Summary and conclusions

According to the IPCC AR4 the geographical patterns of projected surface air temperature warming show greatest temperature increases over land (roughly twice the global average temperature increase) and at high northen latitudes, and less warming over the southern oceans and North Atlantic, consistent with observations during the latter part of the 20th century. The developed simple climate model that only considers simplified representations of central feedback emchanisms in the climate system is indeed able to reproduce the major features of this global surface warming pattern. The global average temperature change lies well within the range suggested by current IPCC models, suggesting that the basic physics explain most of that pattern. Local deviations betwen the simple model result and that of the multi-model mean response of IPCC models lie within the range of single GCMs, since most complex models differ from the ensemble mean as well.

Several experiments were undertaken in order to show the effects of single feedback mechanisms in combination with each other. The known effects of positive feedbacks, such as water vapor and ice-albedo feedback, and negative feedbacks, such as the latent heat feedback, are acting amplifying and dampening, respectively. The most important feedback mechanism is the water vapor feedback which is roughly doubling the model's sensitivity to external forcing. The ice-albedo feedback is amplifying the temperature change in those regions that experience seasonally varying ice or snow cover. However, several physical processes had to be parameterized in order to keep the model as simple as possible. This, however, leads to model failures in reproducing all details of the complex climate system in response to climate change conditions. Nevertheless, it was not the aim of this work to develop one more climate model that is reproducing just a global warming response but to come up with a simplified model version that allows experimental tests of physical relations. This goal indeed has been achieved.

In conclusion, the developed simple climate model is only appropriate for clearing the most general features of climate change under a global warming scenario with increasing CO2 concentration. But it may be used to study the effect of single feedback processes under very simplified conditions. The low computation time and simple structure of this conceptual model suggest a usage as a 'educational tool'. Further improvement and expansion will certainly lead to more realistic results, which than surely agree to a certain limit with the results of more complex models.

# Bibliography


[1] Adam, Julian (1970). Incorporation of advection of heat by mean winds and by ocean currents in a thermodynamic model for long-range weather prediction. Monthly Weather Review, Vol.98, No. 10, 776

[2] Budyko, M.I. (1968). The effect of solar radiation variations on the climate of the Earth. Tellus, 5

[3] Cess, R.D. And G.L. Potter (1988). A Methodology for Understanding and Intercomparing Atmospheric Climate Feedback Processes in General Circulation Models. Journal of Geophysical Research, 93(D7), 8305-8314.

[4] Cogley, J. Graham (1979). The albedo of water as a function of latitude. Monthly Weather Review, No. 107, 775-781

[5] Cubasch, U., R. Voss, G.C. Hegerl, J. Waszkewitz, T.J.Crowley (1997). Simulation of the influence of solar radiation variations on the global climate with an ocean-atmosphere general circulation model. Climate Dynamics, Vol. 13, No. 11

[6] Cubasch, U. and R. Voss (2000). The influence of total solar irradiance on climate. Space Science Reviews. Vol. 94, No. 1-2

[7] DWD (1987). Allgemeine Meteorologie, Leitfäden für die Ausbildung im Deutschen Wetterdienst Nr. 1

[8] Folland, C.K., T.R. Karl, J.R. Christy, R.A. Clarke, G.V. Gruza, J. Jouzel, M.E. Mann, J. Oerlemans, M.J. Salinger and S.-W. Wang (2001). Observed Climatic Variability and Change. In: Climate Change 2001: The Scientific Basis. Contribution of Working Group I to the Third Assessment Report of the Intergovernmental Panel on Climate Change, ed. J.T. Houghton et al., Cambridge Univ. Press

[9] Gal-Chen, Tzvi, Stephen H. Schneider (1975). Energy balance climate modelling: comparison of radiative and dynamic feedback mechanisms. Tellus

[10] Hicks, B.B. (1972). Propeller anemometers as sensors of atmospheric turbulence. Boundary Layer Meteorology, Vol. 3, No. 2

[11] IPCC (2007): Climate Change 2007: The Physical Science Basis. Contribution of Working Group I to the Fourth Assessment Report of the Intergovernmental Panel on Climate Change [Solomon, S., D. Qin, M. Manning, Z. Chen, M. Marquis, K.B. Averyt, M. Tignor and H.L. Miller (eds.)]. Cambridge University Press, Cambridge, United Kingdom and New York, NY, USA, 996 pp. Joshi, 2007: Mechanisms for the land/sea warming contrast exhibited by simulations of climate change

[12] Kent, E.C. And P.K. Taylor (1995). A comparison of sensible and latent heat flux estimates for the North Atlantic ocean. Journal of Physical Oceanography, 25(6), 1530-1549

[13] Kiehl, J.T., K.E. Trenberth (1997). Earth's Annual Global Mean Energy Budget. Bull. Amer. Meteor. Soc., 78, 197-208

[14] Kondo, Junsei (1975). Air-sea bulk transfer coefficients in diabatic conditions. Boundary Layer Meteorology, Vol. 9

[15] Kondo, Junsei and Hiromi Yamazawa (1986). Bulk transfer coefficient over a snow surface. Boundary Layer Meteorology, Vol. 34

[16] Kondo, Junsei, Nobuko Saigusa, Takeshi Sato (1990). A parameterization of evaporation from bare soil surfaces. Journal of Applied Meteorology, Vol. 29, 385-389

[17] Lean, Judith and David Rind (1998). Climate Forcing by Changing Solar Radiation. Journal of Climate, Vol. 11

[18] Lian, M.S. And R.D. Cess (1977). Energy balance climate models: a reappraisal of ice-albedo feedback. Journal of the Atmospheric Sciences, Vol. 34

[19] London, J. and T. Sasamori (1971). Radiative energy budget of the atmosphere. Space Research XI, Vol. 1, pp. 639-649

[20] Lorenz, Edward N. (1968). Three Approaches to Atmospheric Predictability. Bulletin of the American Meteorological Society, Vol. 50, No. 5

[21] Lorenz , Edward N. (1970). Climatic Change as a Mathematical Problem. Journal of Applied Meteorology, Vol. 9

[22] Manabe, Syukuro and Richard T. Wetherald (1967). Thermal equilibrium of the atmosphere with a given distribution of relative humidity. Journal of the Atmospheric Sciences, Vol. 24, No. 3, 241

[23] Manabe, S. , R.J. Stouffer, M.J. Spelman, K. Bryan (1991). Transient responses of a coupled ocean-atmosphere-land surface model to gradual changes of atmospheric CO2. In: Global Change, Proceedings of the first Demetra meeting held at Chianciano Terme, Italy from 28 to 31 October 1991. Environment and Quality of Life, EUR 15158 EN, Directorate-General Science, Research and Development, EuropeanCommission, 82-93

[24] Milankovitch, M. (1941). Kanon der Erdbestrahlung und seine Anwendung auf das Eiszeiten-Problem. Royal Serbian Academy, Belgrade

[25] North, Gerald R. (1975). Theory of energy balance climate models, Journal of the Atmospheric Sciences, Vol. 32, No. 11, 2033

[26] North, Gerald R., Robert F. Cahalan, James A. Coakley, Jr. (1981). Energy balance climate models. Reviews of Geophysics and Space Physics, Vol. 19, No. 1, 91-121

[27] North, Gerald R. (1988). Lessons from energy balance models. Physically-based modelling and simulation of climate and climatic change - Part II, M.E. Schlesinger (ed.), Kluwer Academic Publishers

[28] Ramasway, V. , O. Boucher, I. Haigh, D. Hauglustaine, I. Haywood, G. Myhre, T. Nakajima, G. Shi, S. Solomon, R.E. Betts, R. Charlson, C.C. Chuang, I.S. Daniel, A. D. Del Genio, I. Feichter, I. Fuglestvedt, P.M. Forster, S.I. Ghan, A. Jones, J.T. Kiehl, D. Koch, C. Land, I. Lean, U. Lohmann, K. Minschwaner, J.E. Penner, D.L. Roberts, H. Rodhe, G.-J. Roelofs, L.D. Rotstayn, T.L. Schneider, U. Schumann, S.E. Schwartz, M.D. Schwartzkopf, K.P. Shine, S.J. Smith, D.S. Stevenson, F. Stordal, I. Tegen, R. van Dorland, Y.Zhang, J. Srinivasan, F. Joos (2001). Radiative Forcing of Climate Change. In: Climate Change 2001: The Scientific Basis. Contribution of Working Group I to the Third Assessment Report of the Intergovernmental Panel on Climate Change, ed. J.T. Houghton et al., Cambridge Univ. Press

[29] Rapti, A.S. (2005). Spectral optical atmospheric thickness dependence on the specific humidity in the presence of continental and maritime air masses. Atmospheric Research, Vol. 78

[30] Raschke, E., T.H. Vonder Haar, M. Pasternak and W.R. Bandeen (1973). The radiation balance of the earth-atmosphere system from Nimbus-3 radiation measurements. [NASA TN D-7249]

[31] Schneider, Stephen H., Robert E. Dickinson (1974). Climate modeling. Reviews of Geophysics and Space Physics, Vol. 12, No. 3, 447

[32] Sellers, William D. (1965). Physical Climatology. Chicago. The University of Chicago Press.

[33] Sellers, William D. (1969): A global climate model based on the energy balance of the earth-atmosphere system. Journal of Applied Meteorology, Vol. 8, 392

[34] Sellers, William D. (1973). A new global climate model. Journal of Applied Meteorology, Vol. 12, No. 2, 241

[35] Sutton, Rowan T., Buwen Dong, Jonathan M. Gregory (2007). Land/sea warming ratio in response to climate change: IPCC AR4 model results and comparison with observations. Geophysical Research Letters, Vol. 34, L02701

[36] Wetherald, R.T. And S. Manabe (1975). The effects of chnaging the solar constant on the climate of a general circulation model. Journal of the Atmospheric Sciences, 32(11), 2044-2059

[37] Wetherald, R.T. And S. Manabe (1988). Cloud feedback processes in a general circulation model. Journal of the Atmospheric Sciences, 45(8), 1397-1415

# Danksagung

Bei Prof. Dr. Dietmar Dommenget bedanke ich mich für das Angebot, diese Thema zu bearbeiten, und für seine enorm lehrreiche Betreuung und Unterstützung bei der Umsetzung des Modells. Seine konstruktive Kritik und die vielen wissenschaftlichen Anregungen haben wesentlich zu dieser Arbeit beigetragen. Vielen Dank!

Für die technische und moralische Unterstützung danke ich Björn 'SK' Blöhdörn. Ihm danke ich auch dafür, dass er die Risiken und Nebenwirkungen einer Diplomarbeit mit mir durchgestanden hat. Danke!

Herzlicher Dank gebührt Markus Scheinert und Christina Roth für die Bereitschaft, immer zur Stelle zu sein, wenn ich was loswerden musste und für den enorm Rückhalt, den sie mir gegeben haben. Ihr seid echt gute Freunde!

Besonderer Dank gilt meinen Eltern Andrea und Richard Flöter, ohne deren Unterstützung dieses Studium nur wesentlich schwerer möglich gewesen wäre.

Ein letzter Dank geht an Luko: Danke, dass du mich so oft von der Arbeit abgehalten und mich an die frische Luft gebracht hast!

# Erklärung

Hiermit bestätige ich, dass ich die vorliegende Diplomarbeit selbstständig verfasst und keine anderen als die angegebenen Quellen und Hilfsmittel verwendet habe.

Ich versichere, dass diese Arbeit noch nicht zur Erlangung eines Diplomgrades an anderer Stelle vorgelegen hat.

Kiel, 04.02.09

Janine Flöter